

# Réactions de dissociation: aspects théoriques

Daniel Baye

*Physique Quantique, C.P. 165/82, et*

*Physique Nucléaire Théorique et Physique Mathématique, C.P. 229,*

*Université Libre de Bruxelles (ULB), B1050 Brussels, Belgium*

## Résumé

Les réactions de dissociation sont un des principaux outils pour l'étude de noyaux de courte durée de vie. En particulier, la dissociation coulombienne permet d'obtenir des informations sur les propriétés spectroscopiques des noyaux à halo et sur les facteurs astrophysiques de réactions de capture radiative. Les études les plus simples sont basées sur la théorie des perturbations et en particulier sur son premier ordre. Cependant, la validité de l'approximation du premier ordre peut être limitée pour des systèmes étendus comme les noyaux à halo et ses conditions ne sont pas toujours satisfaites dans les expériences existantes. Des modèles plus élaborés sont disponibles: résolution de l'équation de Schrödinger semi-classique dépendant du temps, approximations eikonale et eikonale dynamique, méthode des voies couplées avec un continu discrétisé (CDCC). Ces méthodes sont passées en revue et résumées. Leur intérêt et leurs limitations sont discutés. Les dissociations du  $^{11}\text{Be}$  et du  $^8\text{B}$  sont traitées comme exemples de ces diverses approximations.

## Abstract

Breakup reactions are one of the main tools for the study of exotic nuclei. In particular, Coulomb breakup is expected to provide information on spectroscopic properties of halo nuclei and on astrophysical  $S$  factors for radiative-capture reactions. The simplest studies are based on perturbation theory and especially on its first order. However the validity of the first-order approximation may be limited for extended systems such as halo nuclei and its conditions are not always satisfied in existing experiments. More elaborate reaction models are available: resolution of the semi-classical time-dependent Schrödinger equation, eikonal and dynamical eikonal approximations, method of coupled discretized-continuum channels (CDCC). These methods are reviewed and summarized. Their interest and limitations are discussed. The  $^{11}\text{Be}$  and  $^8\text{B}$  breakups are treated as examples of the various approximations.

# 1 Introduction

The short lifetime of exotic nuclei does not allow many techniques of analysis. One possibility is to study their decay products. Another possibility compatible with their in-flight production is to collide them with some target nucleus [1-4]. Because of their fragility due to low binding energies, one of the main decay channels is usually the breakup channel. Breakup is a dissociation of the projectile into two or more fragments caused by the interaction with the target nucleus. Here we are interested in breakup processes where the target state remains unchanged (also called elastic breakup or diffractive breakup [5]).

The goal of such experiments is to deduce properties of the projectile initial bound state from the measurement of fragment distributions. Indeed, during the collision process forces act differently on the constituents of the projectile if it displays some amount of clusterization, i.e. if it can be considered as containing subentities grouping several nucleons. The distribution of emitted fragments provides information on this cluster structure of the projectile. However final-state interactions, i.e. interactions between the fragments after the breakup has occurred, may make the interpretation unclear.

An important particular case is Coulomb breakup where the collision can be considered as distant enough so that the nuclear interactions between projectile and target can be neglected. This can be realized for the breakup in the Coulomb field of a heavy nucleus when the scattering angles are small enough. This process is particularly interesting because it provides information on the electromagnetic transition properties of the projectile into the continuum. Moreover Coulomb breakup provides an indirect technique of measurement of cross sections for radiative-capture reactions of astrophysical interest [6, 7].

The analysis of experimental data on breakup reactions inevitably requires the use of some theoretical model [8]. The theoretical description of breakup is difficult because it is a many-body problem in the continuum, both for the initial and final states. Even the simplest case that we study in the following involves three particles in the final channel and thus requires solving a three-body Schrödinger equation in the continuum in the presence of Coulomb forces. This problem thus also requires approximations in the treatment of the reaction mechanism. The aim of the present review is to describe and discuss some of the most efficient reaction descriptions applied in breakup models.

In section 2, we recall some basics of two-body scattering theory and present the three-body model on which various approximate reaction descriptions will be applied. Section 3 is devoted to semi-classical approximations. Purely quantal approximations are described in section 4. Finally, section 5 contains concluding comments.

This text is adapted from Ref. [9].

## 2 Three-body breakup model

### 2.1 Two-body bound and scattering states of the projectile

In breakup reactions of loosely bound systems, the projectile is usually broken into very specific fragments. One can consider that a cluster structure preexists dominantly in the projectile. Such a structure may be described in a microscopic way where

all nucleons are taken into account. However, most present breakup calculations are based on a much simpler description where the internal structure of the fragments is neglected. Internal effects are simulated by the phenomenological interactions between the clusters. The probability of the considered cluster structure in the ground-state wave function of the projectile is simulated by a phenomenological multiplicative factor called *spectroscopic factor*.

Here we assume that the projectile P is made of two structureless clusters. Its two components will be called the core (c) with mass  $m_c$  and charge  $Z_c e$  and fragment (f) with mass  $m_f$  and charge  $Z_f e$ . The internal structure of P can thus be described by the two-body effective potential acting between these clusters. After separation of the centre-of-mass motion, its Hamiltonian for the internal motion reads

$$H_0 = \frac{p^2}{2\mu_{cf}} + V_{cf}(r), \quad (2.1)$$

where  $\mathbf{r}$  and  $\mathbf{p}$  are the relative coordinate and momentum and  $\mu_{cf} = m_c m_f / m_P$  is the core-fragment reduced mass ( $m_P = m_c + m_f$ ). The real effective potential  $V_{cf}$  between core and fragment may depend on the orbital momentum of the relative motion and may contain spin-orbit terms. In the following, we do not consider spin-orbit effects for simplicity.

At negative energies  $E_{nl} < 0$ , bound-state wave functions  $\phi_{nlm}$  verify

$$H_0 \phi_{nlm}(\mathbf{r}) = E_{nl} \phi_{nlm}(\mathbf{r}) \quad (2.2)$$

where  $n$  is the radial quantum number,  $l$  is the orbital momentum and  $m$  is its projection. They satisfy the orthonormality property

$$\langle \phi_{nlm} | \phi_{n'l'm'} \rangle = \delta_{nn'} \delta_{ll'} \delta_{mm'}. \quad (2.3)$$

In spherical coordinates, they factorize as

$$\phi_{nlm}(\mathbf{r}) = r^{-1} Y_l^m(\Omega) u_{nl}(r) \quad (2.4)$$

where  $\Omega = (\theta, \varphi)$  represents the angular variables. The radial wave functions  $u_{nl}$  decrease asymptotically as

$$u_{nl}(r) \xrightarrow{r \rightarrow \infty} N_{nl} \exp(-\kappa_{nl} r) \quad (2.5)$$

where  $\kappa_{nl} = \sqrt{2\mu_{cf}|E_{nl}|}/\hbar$  and  $N_{nl}$  is the asymptotic normalization constant (ANC).

At positive energies  $E > 0$ , scattering wave functions  $\phi_{klm}$  for a given partial wave  $l$  verify

$$H_0 \phi_{klm}(\mathbf{r}) = E \phi_{klm}(\mathbf{r}) \quad (2.6)$$

where the wavenumber  $k$  is given by  $E = \hbar^2 k^2 / 2\mu_{cf}$ . Scattering states are not square-integrable but their normalization can be fixed in different ways. Here we choose a wavenumber normalization defined by

$$\langle \phi_{klm} | \phi_{k'l'm'} \rangle = \delta(k - k') \delta_{ll'} \delta_{mm'}. \quad (2.7)$$

These states are orthogonal for  $k \neq k'$  and their normalization is fixed by a Dirac delta function of  $k - k'$ . They are orthogonal to the bound states,  $\langle \phi_{klm} | \phi_{n'l'm'} \rangle = 0$ . Together with the bound states, the partial-wave scattering wave functions verify the closure relation

$$\sum_{nlm} |\phi_{nlm}\rangle \langle \phi_{nlm}| + \sum_{lm} \int_0^\infty |\phi_{klm}\rangle \langle \phi_{klm}| dk = 1. \quad (2.8)$$

Partial scattering waves can be factorized as [10]

$$\phi_{klm}(\mathbf{r}) = r^{-1} Y_l^m(\Omega) u_{kl}(r). \quad (2.9)$$

The radial functions  $u_{kl}$  are real bounded solutions of the differential equations

$$\left( \frac{d^2}{dr^2} - \frac{l(l+1)}{r^2} - \frac{2\mu_{cf} V_{cf}(r)}{\hbar^2} + k^2 \right) u_{kl}(r) = 0 \quad (2.10)$$

with the initial condition  $u_{kl}(0) = 0$ . Except for a normalization factor, these solutions are unique at given energy. With (2.7), this factor is fixed by

$$\int_0^\infty u_{kl}(r) u_{k'l}(r) dr = \delta(k - k'). \quad (2.11)$$

The asymptotic behaviour of the radial scattering waves is

$$u_{kl}(r) \xrightarrow{r \rightarrow \infty} \sqrt{\frac{2}{\pi}} [\cos \delta_l F_l(\eta, kr) + \sin \delta_l G_l(\eta, kr)] \quad (2.12)$$

$$\xrightarrow{r \rightarrow \infty} \sqrt{\frac{2}{\pi}} \sin(kr - \frac{1}{2}l\pi - \eta \ln 2kr + \sigma_l + \delta_l) \quad (2.13)$$

where  $F_l$  and  $G_l$  are the regular and irregular Coulomb functions [11] depending on the Sommerfeld parameter  $\eta = Z_c Z_f e^2 / \hbar v_{cf}$  ( $v_{cf}$  is the core-fragment relative velocity). The energy-dependent phase shift  $\delta_l$  is due to the effect of potential  $V_{cf}$ . At very large distances, the oscillatory behaviour (2.13) of the radial wave function is distorted by the long-range Coulomb force through the varying phase  $-\eta \ln 2kr$  and the Coulomb phase shift  $\sigma_l = \arg \Gamma(l + 1 + i\eta)$ . These corrections vanish when the fragment is a neutron ( $Z_f = 0$ ).

Collision theory requires other types of states, known as the *stationary scattering states* [10], which are also bounded solutions of the Schrödinger equation at energy  $E$ ,

$$H_0 \phi_{\mathbf{k}}^{(\pm)}(\mathbf{r}) = E \phi_{\mathbf{k}}^{(\pm)}(\mathbf{r}). \quad (2.14)$$

The outgoing stationary scattering states  $\phi_{\mathbf{k}}^{(+)}$  present the asymptotic behaviour

$$\phi_{\mathbf{k}}^{(+)}(\mathbf{r}) \xrightarrow{r \rightarrow \infty} (2\pi)^{-3/2} \left( e^{i(\mathbf{k} \cdot \mathbf{r} + \dots)} + f_{\mathbf{k}}(\Omega) \frac{e^{i(kr + \dots)}}{r} \right) \quad (2.15)$$

involving a Coulomb-distorted plane wave corresponding to the initial wavevector  $\mathbf{k}$  and an outgoing spherical wave. The dots recall the possible existence of logarithmic

Coulomb terms. The coefficient  $f_k$  modulating the outgoing wave is the *scattering amplitude* at energy  $E$  which provides the elastic cross section

$$\frac{d\sigma}{d\Omega} = |f_k(\Omega)|^2. \quad (2.16)$$

The ingoing stationary scattering states  $\phi_{\mathbf{k}}^{(-)}$  are obtained from the outgoing ones by the time reversal operation

$$\phi_{\mathbf{k}}^{(-)}(\mathbf{r}) = \left(\phi_{-\mathbf{k}}^{(+)}(\mathbf{r})\right)^*. \quad (2.17)$$

They thus display the asymptotic behaviour

$$\phi_{\mathbf{k}}^{(-)}(\mathbf{r}) \xrightarrow{r \rightarrow \infty} (2\pi)^{-3/2} \left( e^{i(\mathbf{k} \cdot \mathbf{r} + \dots)} + f_k^*(\Omega) \frac{e^{-i(kr + \dots)}}{r} \right) \quad (2.18)$$

characterized by an ingoing spherical wave and a plane wave representing a final motion in direction  $\mathbf{k}$ . While  $\phi_{\mathbf{k}}^{(+)}$  is associated with initial scattering states,  $\phi_{\mathbf{k}}^{(-)}$  will be useful to describe final breakup states. Both types of states satisfy the orthogonality and normalization properties

$$\langle \phi_{\mathbf{k}}^{(\pm)} | \phi_{\mathbf{k}'}^{(\pm)} \rangle = \delta(\mathbf{k} - \mathbf{k}') \quad (2.19)$$

with a normalization imposing the factor  $(2\pi)^{-3/2}$  in Eqs. (2.15) and (2.18). These states also satisfy closure relations together with the bound states,

$$\sum_{nlm} |\phi_{nlm}\rangle \langle \phi_{nlm}| + \int |\phi_{\mathbf{k}}^{(\pm)}\rangle \langle \phi_{\mathbf{k}}^{(\pm)}| d\mathbf{k} = 1. \quad (2.20)$$

The stationary scattering states can not easily be constructed explicitly. It is thus convenient to expand them in partial waves. Since they are solutions of the same equation at the same energy, they can be expressed as a function of the  $\phi_{klm}$  defined with (2.6) and (2.7) according to

$$\phi_{\mathbf{k}}^{(\pm)}(\mathbf{r}) = k^{-1} \sum_{lm} i^l Y_l^{m*}(\Omega_k) e^{\pm i(\sigma_l + \delta_l)} \phi_{klm}(\mathbf{r}) \quad (2.21)$$

where  $\Omega_k$  is the direction of  $\mathbf{k}$ . Partial waves of  $\phi_{\mathbf{k}}^{(\pm)}$  can be defined as

$$\phi_{klm}^{(\pm)}(\mathbf{r}) = k \int Y_l^m(\Omega_k) \phi_{\mathbf{k}}^{(\pm)}(\mathbf{r}) = i^l e^{\pm i(\sigma_l + \delta_l)} \phi_{klm}(\mathbf{r}). \quad (2.22)$$

Their radial parts only differ from the real solutions  $u_{kl}$  of Eq. (2.10) by a phase factor,

$$u_{kl}^{(\pm)}(r) = i^l e^{\pm i(\sigma_l + \delta_l)} u_{kl}(r). \quad (2.23)$$

## 2.2 Three-body Schrödinger equation

The breakup description will take place in a simple three-body model involving three structureless particles. The projectile P described with the two-body model of section

2.1 collides a pointlike target T with mass  $m_T$  and charge  $Z_T e$ . The Hamiltonian of this three-body model reads

$$H = \frac{p_f^2}{2m_f} + \frac{p_c^2}{2m_c} + \frac{p_T^2}{2m_T} + V_{cf} + V_{fT} + V_{cT} \quad (2.24)$$

where  $\mathbf{p}_i$  is the momentum of particle  $i$  and  $V_{ij}$  is some interaction between particles  $i$  and  $j$ . This equation can describe elastic and inelastic scatterings and breakup but can not describe many other processes such as excitation of the core or target. In order to simulate some effects of these missing channels, the core-target interaction  $V_{cT}$  and the fragment-target interaction  $V_{fT}$  are chosen as complex optical potentials [12]. The imaginary parts of these potentials simulate the disparition of flux from the initial channel.

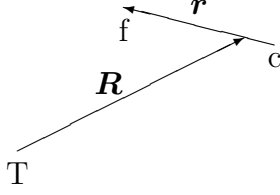


Figure 1: Jacobi coordinates.

In order to solve Eq. (2.24), it is convenient to introduce Jacobi coordinates (see Fig. 1) and their conjugate momenta [13]. In addition to the centre-of-mass coordinate  $\mathbf{R}_{cm}$  and the total momentum  $\mathbf{P}_{cm}$ , one defines the internal projectile coordinate and momentum

$$\mathbf{r} = \mathbf{r}_f - \mathbf{r}_c, \quad \mathbf{p} = \frac{m_c \mathbf{p}_f - m_f \mathbf{p}_c}{m_P} \quad (2.25)$$

and the projectile-target relative coordinate and momentum

$$\mathbf{R} = \frac{m_f \mathbf{r}_f + m_c \mathbf{r}_c}{m_P} - \mathbf{r}_T, \quad \mathbf{P} = \frac{m_T (\mathbf{p}_f + \mathbf{p}_c) - m_P \mathbf{p}_T}{m_P + m_T}. \quad (2.26)$$

The corresponding orbital momenta  $\mathbf{l} = \mathbf{r} \times \mathbf{p}$  and  $\mathbf{L} = \mathbf{R} \times \mathbf{P}$  allow writing the total internal orbital momentum of the three-body system as

$$\mathbf{J} = \mathbf{l} + \mathbf{L}. \quad (2.27)$$

If spins were taken into account, the total angular momentum would be obtained by coupling the total internal orbital momentum with the total spin.

After separation of the centre-of-mass motion, the three-body Schrödinger equation becomes

$$\left( \frac{P^2}{2\mu_{PT}} + H_0 + V_{PT}(\mathbf{R}, \mathbf{r}) \right) \Psi(\mathbf{R}, \mathbf{r}) = E_{\text{tot}} \Psi(\mathbf{R}, \mathbf{r}) \quad (2.28)$$

where  $\mu_{PT}$  is the projectile-target reduced mass and the projectile-target potential is given by

$$V_{PT}(\mathbf{R}, \mathbf{r}) = V_{cT} \left( \mathbf{R} - \frac{m_f}{m_P} \mathbf{r} \right) + V_{fT} \left( \mathbf{R} + \frac{m_c}{m_P} \mathbf{r} \right). \quad (2.29)$$

The main problem is to approximately solve Eq. (2.28) in the continuum.

### 3 Semi-classical approximation

#### 3.1 Time-dependent Schrödinger equation

The semi-classical approximation consists in a quantal description of the internal motion in the projectile and a classical description of the projectile-target relative motion [14]. The reference frame can conveniently be chosen at the centre of mass of the projectile. A trajectory  $\mathbf{R}(t)$  with an impact parameter  $b$  and an initial velocity  $v$  is selected to describe the target motion with respect to the projectile. In order that the notion of trajectory be valid, the reduced de Broglie wavelength  $\hbar/P = 1/K$  must be small with respect to the impact parameter, i.e.,  $Kb \gg 1$ . Since energy is conserved on this trajectory, excitation energies of the projectile should be negligible with respect to the projectile energy. Because the nuclear interaction is complex in an optical potential, its effect is usually not taken into account in the choice of a trajectory. The trajectory is thus in general a Rutherford hyperbola due to Coulomb effects only (see Appendix A), or even a straight line if only small scattering angles are considered.

The target motion induces a time-dependent potential acting on the projectile [15-26]. If  $\mathbf{R}(t)$  represents the trajectory of the target with respect to the projectile, the evolution of the system is given by the time-dependent Schrödinger equation

$$i\hbar\frac{\partial}{\partial t}\Psi(\mathbf{r}, t) = [H_0 + V(\mathbf{r}, t)]\Psi(\mathbf{r}, t) \quad (3.1)$$

where the time-dependent potential  $V$  is defined by

$$V(\mathbf{r}, t) = V_{PT}(\mathbf{R}(t), \mathbf{r}) - \frac{(Z_c + Z_f)Z_T e^2}{R(t)}. \quad (3.2)$$

The last term in this expression compensates the fact that the particle follows a Coulomb trajectory and that a Coulomb potential is already included in the trajectory definition. As it does not depend on  $\mathbf{r}$ , its effect is just modifying the phase of the wave function. It can thus be included or omitted without modifying the physical results. The solution of Eq. (3.1) can be formally written as

$$\Psi(\mathbf{r}, t) = U(t, t_0)\Psi(\mathbf{r}, t_0) \quad (3.3)$$

where  $U$  is the evolution operator from  $t_0$  to  $t$ . Operator  $U$  is unitary if  $V$  is real. The initial condition is fixed by

$$\Psi(\mathbf{r}, t_0) \xrightarrow[t_0 \rightarrow -\infty]{} e^{-iE_0 t_0/\hbar}\phi_0(\mathbf{r}) \quad (3.4)$$

where  $\phi_0$  is the ground-state wave function of  $H_0$  and the phase factor arises from Eq. (3.1) when  $V$  is negligible. The physics of the reaction is deduced from the wave function at  $+\infty$ .

#### 3.2 Cross sections

Here and in the following, we assume for simplicity that the system has a single bound state. The probability that the system remains in its ground state with wave function  $\phi_0$  is

$$P_0 = |\langle\phi_0|\Psi(+\infty)\rangle|^2 \quad (3.5)$$

Hence, the elastic cross section is given by

$$\frac{d\sigma}{d\Omega} = \frac{d\sigma_R}{d\Omega} P_0(b) \quad (3.6)$$

where the Rutherford cross section

$$\frac{d\sigma_R}{d\Omega} = |f_C(\Omega)|^2 = \frac{\eta^2}{4k^2 \sin^4 \frac{1}{2}\theta} \quad (3.7)$$

is obtained from the Coulomb scattering amplitude  $f_C$  [Eq. (4.27)]. To make sense, Eq. (3.6) must be complemented by a relation between the scattering angle  $\theta$  and the impact parameter  $b$ , such as relation  $b = a \cot \frac{1}{2}\theta$  valid for a Coulomb trajectory, where  $a = \eta/k$  is half the distance of closest approach in head-on collisions (see Appendix A).

The breakup momentum distribution is given by

$$\frac{dP}{d\mathbf{k}} = \left| \langle \phi_{\mathbf{k}}^{(-)} | \Psi(+\infty) \rangle \right|^2 \quad (3.8)$$

where  $\phi_{\mathbf{k}}^{(-)}$  is a solution of the Schrödinger equation (2.14) with asymptotic behaviour defined by (2.18). The corresponding cross section reads

$$\frac{d\sigma}{d\mathbf{k}} = 2\pi \int_0^\infty b db \frac{dP}{d\mathbf{k}}. \quad (3.9)$$

The total probability is obtained from the closure relation (2.20) as

$$P_0 + \int \frac{dP}{d\mathbf{k}} d\mathbf{k} = \langle \Psi(+\infty) | \Psi(+\infty) \rangle. \quad (3.10)$$

If all potentials are real, these probabilities sum up to one. Because of absorption in  $V_{cT}$  and  $V_{fT}$ , the norm of  $\Psi(+\infty)$  and thus the sum are smaller than unity.

Expression (3.8) can be expanded in partial waves with (2.21) as

$$\frac{dP}{d\mathbf{k}} = k^{-2} \left| \sum_{lm} (-i)^l Y_l^m(\Omega_k) e^{i(\sigma_l + \delta_l)} \langle \phi_{klm} | \Psi(+\infty) \rangle \right|^2 \quad (3.11)$$

where  $\phi_{klm}$  is defined by (2.9). After integration over the direction  $\Omega_k$  of emission of the fragments, one obtains the momentum distribution

$$\frac{dP}{dk} = k^2 \int d\Omega_k \frac{dP}{d\mathbf{k}} = \sum_{lm} |\langle \phi_{klm} | \Psi(+\infty) \rangle|^2. \quad (3.12)$$

The energy distribution then reads

$$\frac{dP}{dE} = \left( \frac{dE}{dk} \right)^{-1} \frac{dP}{dk} = \frac{1}{\hbar v_{cf}} \sum_{lm} |\langle \phi_{klm} | \Psi(+\infty) \rangle|^2 \quad (3.13)$$

where  $v_{cf}$  is the relative velocity between core and fragment. Eq. (3.13) leads to the differential cross section with respect to the energy of the relative motion between the projectile fragments

$$\frac{d\sigma}{dE} = 2\pi \int_0^\infty b db \frac{dP}{dE}. \quad (3.14)$$

### 3.3 First-order perturbation theory

The time-dependent Schrödinger equation (TDSE) reads

$$i\hbar \frac{d}{dt} \Psi(t) = [H_0 + V(t)] \Psi(t). \quad (3.15)$$

If the potential is small enough, the first-order perturbation approximation  $\Psi^{(1)}(t)$  of the wave function is obtained by replacing  $\Psi(t)$  in the right-hand side of (3.15) by  $\Psi(-\infty) = e^{-iH_0 t/\hbar} \phi_0$  [Eq. (3.4)]. By projecting on  $|\phi_{klm}\rangle$ , one obtains

$$e^{iEt/\hbar} \langle \phi_{klm} | \Psi^{(1)}(+\infty) \rangle = \frac{1}{i\hbar} \int_{-\infty}^{+\infty} e^{i\omega t} \langle \phi_{klm} | V(t) | \phi_0 \rangle dt, \quad (3.16)$$

with the Bohr frequency  $\omega = (E - E_0)/\hbar$ . This approximation can be used in the probability distribution (3.13) and the cross section (3.14).

### 3.4 Coulomb breakup at first order

In the important particular case of Coulomb breakup, potential (3.2) reads

$$V^C(\mathbf{r}, t) = \frac{Z_c Z_T e^2}{|\mathbf{R}(t) - \frac{m_f}{m_P} \mathbf{r}|} + \frac{Z_f Z_T e^2}{|\mathbf{R}(t) + \frac{m_c}{m_P} \mathbf{r}|} - \frac{(Z_c + Z_f) Z_T e^2}{R(t)}. \quad (3.17)$$

With the von Neuman expansion

$$\frac{1}{|\mathbf{r}' - \mathbf{r}|} = \sum_{\lambda=0}^{\infty} \frac{r_{<}^{\lambda}}{r_{>}^{\lambda+1}} \frac{4\pi}{2\lambda+1} \sum_{\mu=-\lambda}^{\lambda} Y_{\lambda}^{\mu*}(\Omega') Y_{\lambda}^{\mu}(\Omega), \quad (3.18)$$

where  $r_{>} = \max(r, r')$ ,  $r_{<} = \min(r, r')$ , and the far-field approximation  $R > r$ , one obtains

$$V^C(\mathbf{r}, t) \approx Z_T e \sum_{\lambda=1}^{\infty} \frac{4\pi}{2\lambda+1} \sum_{\mu=-\lambda}^{\lambda} \frac{Y_{\lambda}^{\mu*}(\Omega_R)}{R^{\lambda+1}} \mathcal{M}_{\mu}^{(E\lambda)}. \quad (3.19)$$

The electric multipole operators

$$\mathcal{M}_{\mu}^{(E\lambda)} = Z_{\text{eff}}^{(E\lambda)} e r^{\lambda} Y_{\lambda}^{\mu}(\Omega) \quad (3.20)$$

involve the effective charges

$$Z_{\text{eff}}^{(E\lambda)} = Z_c \left( \frac{m_f}{m_P} \right)^{\lambda} + Z_f \left( -\frac{m_c}{m_P} \right)^{\lambda}. \quad (3.21)$$

Effective charges are useful to estimate the importance of the role of the various multipoles. When the fragment is a neutron ( $Z_f = 0$ ), the E2 component is small. For example, for the breakup of  $^{11}\text{Be}$  into  $^{10}\text{Be} + n$ , the E1 charge is  $4/11 \approx 0.36$  and the E2 charge is  $4/121 \approx 0.03$ . The situation is quite different when the fragment is a proton ( $Z_f = 1$ ). For the breakup of  $^8\text{B}$  into  $^7\text{Be} + p$ , the E1 charge is  $3/8 \approx 0.38$  but the E2 charge is larger,  $53/64 \approx 0.83$ .

The scalar products (3.16) become up to an irrelevant phase factor

$$\langle \phi_{klm} | \Psi^{(1)}(+\infty) \rangle \approx \frac{Z_T e}{i\hbar} \sum_{\lambda=1}^{\infty} \frac{4\pi}{2\lambda+1} \sum_{\mu=-\lambda}^{\lambda} \langle \phi_{klm} | \mathcal{M}_{\mu}^{(E\lambda)} | \phi_0 \rangle I_{\lambda\mu} \quad (3.22)$$

with the integrals over time,

$$I_{\lambda\mu} = \int_{-\infty}^{+\infty} e^{i\omega t} \frac{Y_{\lambda}^{\mu*}[\Omega_R(t)]}{R(t)^{\lambda+1}} dt. \quad (3.23)$$

For a straight-line trajectory  $\mathbf{R}(t) = \mathbf{v}t + \mathbf{b}$ , their analytical expression is given from Eq. (15) of Ref. [27] as

$$I_{\lambda\mu} = \frac{1}{v} \sqrt{\frac{2\lambda+1}{\pi}} \frac{i^{\lambda+\mu}}{\sqrt{(\lambda+\mu)!(\lambda-\mu)!}} \left(\frac{\omega}{v}\right)^{\lambda} K_{|\mu|} \left(\frac{\omega b}{v}\right) \quad (3.24)$$

which involves a Hankel function  $K_n(x)$  [11].

For simplicity, we now assume  $l_0 = 0$  and denote the radial wave function of the ground state as  $u_0$ . Selection rules in (3.22) then provide  $\lambda = l$  and  $\mu = m$ . Let us define the dipole strength ( $\lambda = 1$ ) as

$$\frac{dB(E1)}{dE} = \frac{1}{\hbar v_{cf}} \sum_m |\langle \phi_{k1m} | \mathcal{M}_m^{(E1)} | \phi_0 \rangle|^2 = \frac{3(Z_{\text{eff}}^{(E1)} e)^2}{4\pi \hbar v_{cf}} \left| \int_0^{\infty} u_{k1}(r) r u_0(r) dr \right|^2. \quad (3.25)$$

With (3.24), the probability distribution (3.13) of dipole breakup of the projectile P into core c and fragment f reads at first order

$$\frac{dP^{(1)}(E1)}{dE} = \frac{16\pi}{9} \left(\frac{Z_T e}{\hbar v}\right)^2 \left(\frac{\omega}{v}\right)^2 [K_0(x)^2 + K_1(x)^2] \frac{dB(E1)}{dE} \quad (3.26)$$

where  $x = \omega b/v$ . The electric dipole breakup cross section is given by

$$\frac{d\sigma^{(1)}(E1)}{dE} = 2\pi \int_{b_{\min}}^{\infty} b db \frac{dP^{(1)}(E1)}{dE}, \quad (3.27)$$

where the smallest impact parameter  $b_{\min}$  corresponds to the maximum scattering angle in the experiment. With the integral

$$\int x K_n^2(x) dx = \frac{1}{2} x^2 [K_n^2(x) - K_{n-1}(x) K_{n+1}(x)] \quad (3.28)$$

and recurrence relations [11], it can be written as

$$\frac{d\sigma^{(1)}(E1)}{dE} = \frac{32\pi^2}{9} \left(\frac{Z_T e}{\hbar v}\right)^2 x_{\min} K_0(x_{\min}) K_1(x_{\min}) \frac{dB(E1)}{dE} \quad (3.29)$$

with  $x_{\min} = \omega b_{\min}/v$ . When the first-order perturbation and far-field approximations are valid, a measurement of the breakup cross section provides the electric dipole strength which in turn provides the cross section for the radiative-capture process  $c(f, \gamma)P$  [6]

$$\sigma_{\gamma}(E1) \propto \frac{dB(E1)}{dE} \quad (3.30)$$

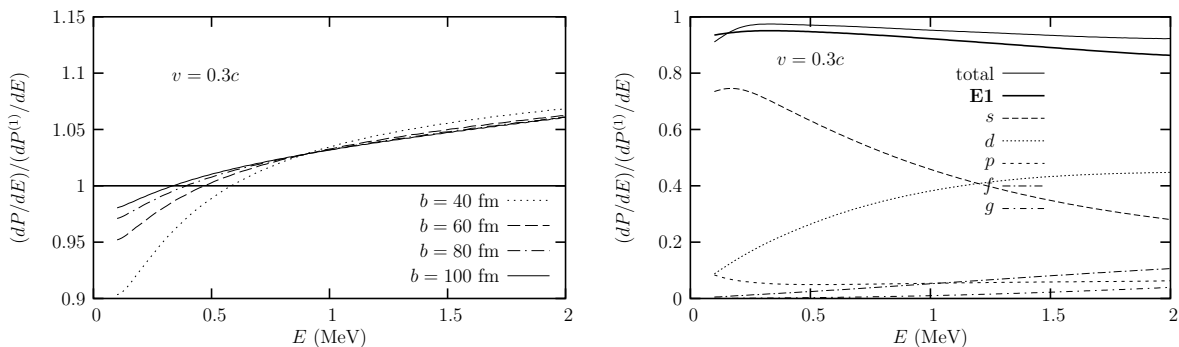


Figure 2: Accuracy of first-order perturbation theory for  $^{11}\text{Be}$  breakup in the left panel and  $^8\text{B}$  breakup in the right panel (adapted from Ref. [30]).

(see Refs. [28, 29] for a detailed expression of  $\sigma_\gamma$ ). The validity of the simple first-order approximation is however limited, even at large impact parameters as shown by Fig. 2.

In Fig. 3 are shown ratios of breakup probability distributions calculated by solving the time-dependent Schrödinger equation (see section 3.5) to the corresponding first-order quantities at large impact parameters [30]. The  $^{11}\text{Be}$  breakup is presented in the left panel. One observes that even at very large impact parameters, the first-order E1 approximation does not reproduce the time-dependent results. The accuracy is about 5 %. Moreover the energy dependence is different. For the  $^8\text{B}$  breakup presented in the right panel, the first-order result contains both E1 and E2 components. The ratio is always smaller than unity.

A simple analytical approximation exists for the dipole strength of a bound neutron [13, 31]. Let us use it to illustrate a technique of determination of the spectroscopic factor  $S$ . The scattering wave  $\phi_{klm}$  is approximated by a partial wave  $k\sqrt{2/\pi}j_l(kr)Y_l^m(\Omega)$  of a plane wave and the initial ground-state wave function  $\phi_0$  by its asymptotic behaviour  $N_0r^{-1}e^{-\kappa_0r}Y_0^0(\Omega)$  [Eq. (2.5)]. A simple integration in (3.25) using  $j_1 = -j_0'$  leads to

$$\frac{dB(\text{E1})}{dE} = \frac{3}{\pi^2}(Z_{\text{eff}}^{(\text{E1})}e)^2 \frac{\hbar^2}{\mu_{cf}E_0^2} \frac{SN_0^2}{2\kappa_0} f\left(\frac{E}{|E_0|}\right) \quad (3.31)$$

where a spectroscopic factor  $S$  is introduced as explained in section 2.1 to simulate the fact that the projectile does not have a pure core-neutron structure. Function  $f$  is given by

$$f(x) = \frac{x^{3/2}}{(x+1)^4}. \quad (3.32)$$

It has a maximum at  $x = 3/5$  so that, according to this simple model, the dipole strength can be expected to be maximum near  $E = 3|E_0|/5$ . The shapes of the dipole strength and of the breakup cross section are thus very sensitive to the value of the ground-state energy for weakly bound systems.

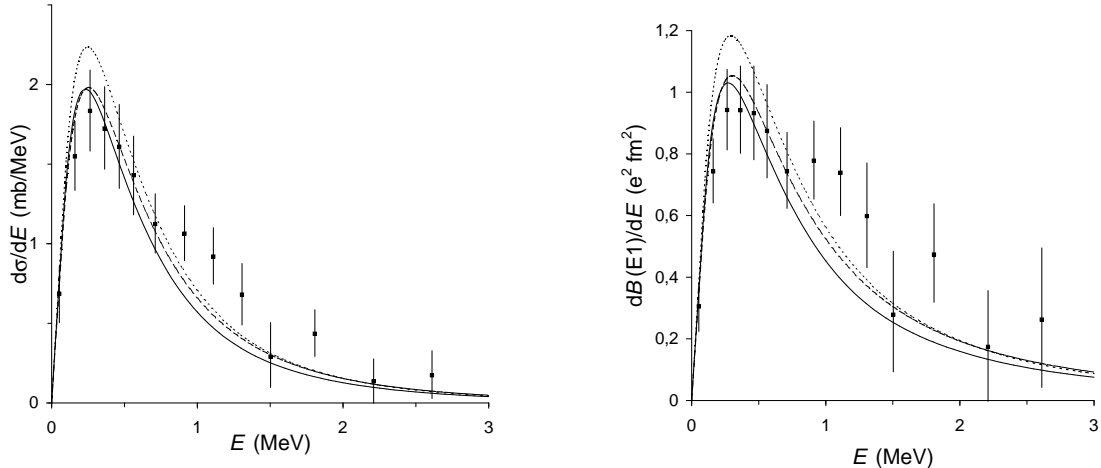


Figure 3: Breakup cross section (left,  $b_{\min} = 13$  fm) and E1 strength (right) for the  $^{11}\text{Be}$  breakup on  $^{208}\text{Pb}$  at 72 MeV/nucleon obtained with Saxon-Woods potentials of Ref. [26] without spin-orbit term (full lines) and of Ref. [33] (dotted lines) and with Eq. (3.31) (dashed lines). Experimental data from Ref. [32].

As an example, we consider the  $^{11}\text{Be}$  breakup. The  $^{11}\text{Be}$  one-neutron halo nucleus possesses two weakly bound states: a  $1/2^+$  ( $l = 0$ ) ground state with a neutron separation energy  $S_n = 0.503$  MeV and a  $1/2^-$  ( $l = 1$ ) excited state with  $S_n = 0.183$  MeV. In Fig. 3, the maximum of the experimental E1 strength of Ref. [32] is located near 0.3 MeV, as expected from the simple model (3.31). Let us now describe and discuss the determination of the spectroscopic factor performed in Ref. [32]. In Ref. [32], the ANC in Eq. (3.31) is deduced from the ground-state wave function in a square well with radius 4 fm, which provides  $N_0 = 0.783 \text{ fm}^{-1/2}$ . As shown by the dashed curves in Fig. 3, a fit of the RIKEN data leads to  $S \approx 1$  [32]. However, expression (3.31) should be replaced by a more realistic calculation involving a potential. Let us use Saxon-Woods potentials to calculate the radial wave functions appearing in (3.25). The potential of Ref. [26] (adapted from Ref. [20]) reproduces the two bound states of  $^{11}\text{Be}$ . Here we neglect the spin-orbit term for simplicity. The potential  $-V_0/[1 + \exp((r - 2.669)/0.6)]$  with  $V_0 = 59.5$  MeV for  $l = 0$  and 40.5 MeV for  $l > 0$  provides the full curves in Fig. 3 which are very close to the dashed curves. With this potential, the ANC is  $0.837 \text{ fm}^{-1/2}$  and the spectroscopic factor is also close to one. However if one uses the potential  $-59.05/[1 + \exp((r - 2.75)/0.62)]$  of Ref. [33] which only reproduces the ground-state energy, the results (dotted lines) are rather different in spite of a similar ANC of  $0.845 \text{ fm}^{-1/2}$ . The deduced spectroscopic factor ( $\approx 0.8$ ) is then smaller with such a potential. The ‘measured’ spectroscopic factor is thus sensitive to the potential choice because the transition strength also depends on the properties of the final scattering state as explained in Ref. [34] with time-dependent (section 3.5) and CDCC (section 4.4) calculations. Since the potential of Ref. [33] does not reproduce the  $l = 1$  weakly bound state, its validity for the  $l = 1$  final scattering state, and hence the derived spectroscopic factor, are dubious.

The interest of working with the E1 strength is that it allows comparing experiments at different energies (provided that the first-order approximation is valid in both cases).

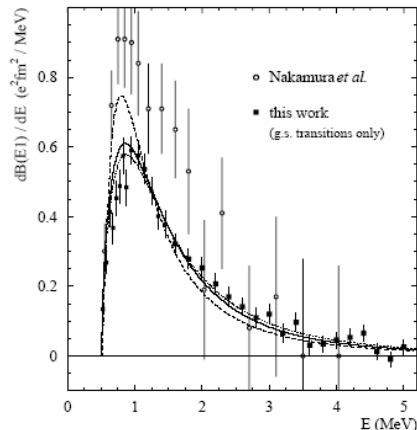


Figure 4: Comparison of E1 strengths from the GSI and RIKEN experiments in 2003 (Fig. 6 from Ref. [35]).

Data for the dipole strength but with a different normalization were obtained at GSI from an experiment at much higher energies [35]. A comparison in Fig. 4 shows that the GSI data taken at 520 MeV/nucleon do not agree with the RIKEN data of that time. The GSI normalization was eventually confirmed at RIKEN [33] following a recalibration [36, 33] and leads to a reduction by a factor 0.85 of the data of Ref. [32]. The spectroscopic factor should thus be reduced accordingly. This reduction and the controversial potential choice in Ref. [33] then lead to a much smaller spectroscopic factor. As shown by this example, determinations of spectroscopic factors may thus be affected by potential choices in a non negligible way. The uncertainty on the  $^{11}\text{Be}$  spectroscopic factor remains rather large, because of the uncertainties on both the data normalization and the potential choice.

### 3.5 Numerical resolution of the TDSE

The TDSE (3.1) is solved from  $-T$  to  $+T$  ( $T$  large) by small time steps  $\Delta t$ . A three-dimensional (3D) representation of the projectile internal wave function is needed. Because of the angular-momentum dependence of the  $V_{cf}$  interaction, it is preferable to use spherical coordinates [17-24, 26, 37-40]<sup>1</sup>. The wave function can be represented on a 3D mesh, as depicted in Fig. 5 [26]. The evolution of the wave function after a time interval  $\Delta t$  is obtained with the evolution operator  $U$  according to Eq. (3.3),

$$\psi(t + \Delta t) = U(t + \Delta t, t)\psi(t). \quad (3.33)$$

For a small enough time step, approximations of this operator can be derived. See references [26, 41, 9] for more information.

The  $^{11}\text{Be}$  breakup on a  $^{208}\text{Pb}$  target has been studied with this technique [24, 26]. In that case, the dissociation is mostly due to the Coulomb interaction. The  $^{11}\text{Be}$  nucleus

<sup>1</sup>Cartesian coordinates are employed in Ref. [25].

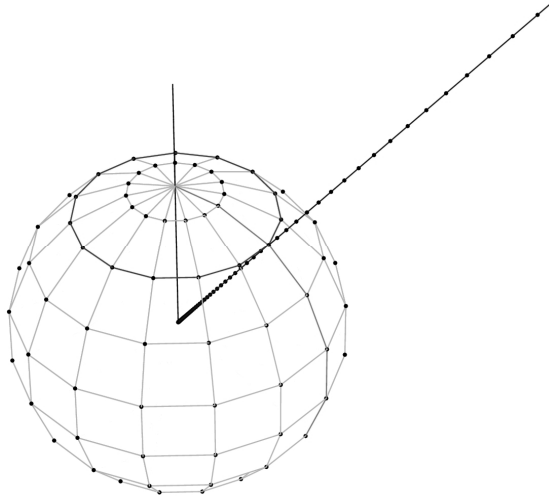


Figure 5: Example of three-dimensional discretization: two-dimensional angular mesh on a sphere and radial mesh.

displays a  $5/2^+$  ( $l = 2$ ) resonance at 1.27 MeV ( $\Gamma = 0.10 \pm 0.02$  MeV) above the  $^{10}\text{Be} + n$  threshold. This resonance is not observed in experiments on heavy targets. On a light  $^{12}\text{C}$  target however, the dashed curve in Fig. 6 shows that a resonance is clearly visible [37]. That it is the  $5/2^+$  resonance is shown by the  $d5/2$  contribution (dotted curve). The resonance is also visible in the experimental data but seems to be much broader. The agreement becomes very good when the theoretical results are convoluted with the experimental resolution (full curve). After the choice of a  $^{10}\text{Be} + n$  potential reproducing the  $^{11}\text{Be}$  properties, the theoretical calculation does not contain any parameter fit. The results are sensitive to the separation energy as shown by the example of the  $^{19}\text{C}$  breakup in Ref. [24].

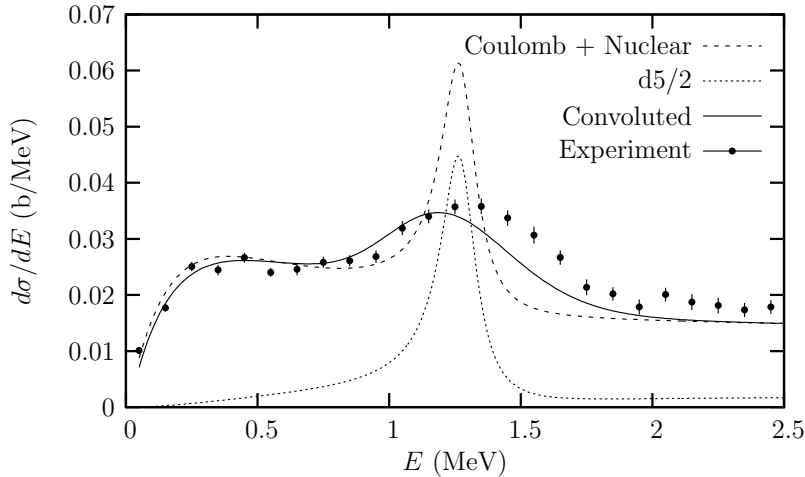


Figure 6: Cross section for the  $^{11}\text{Be}$  breakup on  $^{12}\text{C}$  at 67 MeV/nucleon (adapted from Ref. [37]). Experimental data from Ref. [33].

## 3.6 Summary and comments

First-order perturbation theory shows that, at energies of most experiments, breakup is dominated by the E1 contribution for a neutron halo and by E1+E2 contributions for a proton halo as indicated by the effective charges (3.21). At MSU and RIKEN energies between about 40 and 80 MeV/nucleon, higher-order corrections are not negligible. In particular, a second-order E1-E1 transition may lead to important corrections. Higher-order corrections probably become negligible at GSI energies (around 250 MeV/nucleon) but relativistic effects may then play a role.

Numerical resolutions of the TDSE are accurate but time-consuming. The semiclassical treatment is valid mainly for integrated cross sections. Differential cross sections can not be calculated when a plausible trajectory can not be determined, or are not realistic because interference effects are missing. But we shall see in section 4.3 that it is also the basis of a quantal approximation giving access to angular distributions.

## 4 Quantum approximations

### 4.1 Cross sections

#### General expression

Let us first derive the expression of breakup cross sections by starting from the general non-relativistic expression of a cross section [42, 43],

$$d^{3N}\sigma = \frac{(2\pi)^4}{\hbar v} |\tilde{T}_{fi}|^2 \delta\left(\sum_{f=1}^N E'_f - E_1 - E_2 - Q\right) \delta\left(\sum_{f=1}^N \mathbf{k}'_f - \mathbf{k}_1 - \mathbf{k}_2\right) \left(\prod_{f=1}^N d\mathbf{k}'_f\right). \quad (4.1)$$

This expression describes a reaction with two particles in the entrance channel with initial wavevectors  $\mathbf{k}_1$  and  $\mathbf{k}_2$  and energies  $E_1$  and  $E_2$ ;  $v$  is the asymptotic initial relative velocity between these particles. The outgoing channel with threshold energy  $Q$  involves  $N$  particles with final wavevectors  $\mathbf{k}'_f$  and energies  $E'_f$  ( $f = 1$  to  $N$ ). The  $3N$ -differential cross section corresponds to a situation where the final particles occupy a volume element  $\prod_{f=1}^N d\mathbf{k}'_f$  of phase space around the directions  $\mathbf{k}'_1, \mathbf{k}'_2, \dots, \mathbf{k}'_N$ . The energy and wavenumber (or momentum) conservation laws are included in the Dirac  $\delta$  functions. Dynamical effects are included in the transition matrix element  $\tilde{T}_{fi}$ .

The  $T$ -matrix element can be defined in several equivalent ways [42, 43]. Here it is a matrix element of the interaction potential. The wave function in the ket is the exact solution of the Schrödinger equation with a normalization such as in Eq. (2.15). The wave function in the bra describes  $N - 1$  free relative motions of the  $N$  final particles.

The general procedure then consists in integrating over the final total momentum  $\mathbf{K}'_{\text{cm}}$ . Momentum conservation is then satisfied. A  $3N - 4$  differential cross section is obtained by integrating over one final energy. This energy can be chosen in various ways and in various reference frames in order to match the conditions of a given experiment. When some variables are not measured, further integrations are necessary.

#### Elastic scattering

Let us first consider the simple example of elastic scattering ( $N = 2$ ). The wavevectors of the final particles (which remain identical to the initial P and T particles) can be

replaced by the total and relative wavevectors

$$\mathbf{K}'_{\text{cm}} = \mathbf{k}'_P + \mathbf{k}'_T, \quad \mathbf{k}' = \frac{m_T \mathbf{k}'_P - m_P \mathbf{k}'_T}{m_P + m_T}. \quad (4.2)$$

Integration over the total wavevector leads to

$$d^3\sigma = \frac{1}{(2\pi)^2 \hbar v} |T_{fi}|^2 \delta\left(\frac{\hbar^2 k'^2}{2\mu_{PT}} - E - Q\right) d\mathbf{k}' \quad (4.3)$$

where factors  $(2\pi)^{-3/2}$  have been explicitly removed from the matrix element  $T_{fi}$ . The transition matrix element is thus now defined as

$$T_{fi} = (2\pi)^3 \tilde{T}_{fi} = \langle e^{i\mathbf{k}' \cdot \mathbf{r}} | V_{PT} | \psi(\mathbf{r}) \rangle. \quad (4.4)$$

It involves the exact scattering wave function of the two-body Hamiltonian normalized as  $\psi(\mathbf{r}) \xrightarrow{z \rightarrow -\infty} e^{i(kz + \dots)}$  where the dots recall the possible existence of Coulomb distortion. With the decomposition in spherical components  $d\mathbf{k}' = k'^2 dk' d\Omega$  and the  $\delta$  function property

$$\delta[f(x) - f(x_0)] = \frac{1}{|f'(x_0)|} \delta(x - x_0), \quad (4.5)$$

the differential elastic cross section becomes

$$\frac{d\sigma}{d\Omega} = \frac{1}{(2\pi)^2} \frac{\mu_{PT}^2}{\hbar^4} |T_{fi}|^2 = |f_k(\Omega)|^2, \quad (4.6)$$

where the last equality arises from (2.16), and  $k' = k$ . Comparing (4.4) with (4.19) below, one verifies that the scattering amplitude is indeed related to the  $T$ -matrix element by

$$f_k(\Omega) = -\frac{\mu_{PT}}{2\pi\hbar^2} T_{fi}. \quad (4.7)$$

## Breakup

Now we consider the more complicated breakup case ( $N = 3$ ). The different final wavevectors can be replaced by the total momentum and the relative momenta (2.25) and (2.26),

$$\mathbf{K}'_{\text{cm}} = \mathbf{k}'_f + \mathbf{k}'_c + \mathbf{k}'_T, \quad \mathbf{K}' = \frac{m_T(\mathbf{k}'_f + \mathbf{k}'_c) - m_P \mathbf{k}'_T}{m_P + m_T}, \quad \mathbf{k} = \frac{m_c \mathbf{k}'_f - m_f \mathbf{k}'_c}{m_P}. \quad (4.8)$$

Notation  $\mathbf{k}$  is preferred to notation  $\mathbf{k}'$  since there is no ambiguity. Integration over the total wavevector leads to

$$d^6\sigma = \frac{1}{(2\pi)^5 \hbar v} |T_{fi}|^2 \delta\left(\frac{\hbar^2 K'^2}{2\mu_{PT}} + \frac{\hbar^2 k^2}{2\mu_{cf}} - E - Q\right) d\mathbf{k} d\mathbf{K}'. \quad (4.9)$$

Three factors  $(2\pi)^{-3/2}$  have been explicitly removed from the transition matrix element defined as

$$T_{fi} = (2\pi)^{9/2} \tilde{T}_{fi} = \langle e^{i\mathbf{K}' \cdot \mathbf{R}} \phi_{\mathbf{k}}^{(-)}(\mathbf{r}) | V_{PT} | \Psi(\mathbf{R}, \mathbf{r}) \rangle \quad (4.10)$$

with the asymptotic normalization

$$\Psi(\mathbf{R}, \mathbf{r}) \xrightarrow{Z \rightarrow -\infty} e^{i(KZ+\dots)} \phi_0(\mathbf{r}) \quad (4.11)$$

and a similar normalization for  $\phi_{\mathbf{k}}^{(-)}$ . If one integrates over the norm of the final relative momentum  $\mathbf{K}' = (K', \Omega)$ , one obtains the 5-differential cross section in the centre-of-mass frame,

$$\frac{d\sigma}{d\mathbf{k}d\Omega} = \frac{1}{(2\pi)^5} \frac{\mu_{PT}K'}{\hbar^3 v} |T_{fi}|^2. \quad (4.12)$$

The derivation of expressions for laboratory cross sections with the above procedure is discussed in Ref. [44]. An example that can be obtained from (4.9) is given by Eqs. (15) and (16) of Ref. [45].

## 4.2 Eikonal approximation

### Potential scattering

Before applying this approximation to breakup, let us consider the simpler case of potential scattering,

$$\left( \frac{p^2}{2\mu} + V(r) \right) \psi = E\psi \quad (4.13)$$

According to Ref. [46], the wave function is factorized as

$$\psi(\mathbf{r}) = e^{ikz} \hat{\psi}(\mathbf{r}). \quad (4.14)$$

With the velocity  $v = \hbar k / \mu$ , the Schrödinger equation becomes

$$\left( \frac{p^2}{2\mu} + vp_z + V(r) \right) \hat{\psi} = 0. \quad (4.15)$$

This is still an exact expression. At high energy, the new function  $\hat{\psi}$  is expected to verify

$$|\Delta \hat{\psi}| \ll k |\nabla \hat{\psi}| \quad (4.16)$$

since  $k$  is large. Most of the wave function variation is included in factor  $e^{ikz}$ . Hence, Eq. (4.15) can be approximated as

$$\left( -i\hbar v \frac{\partial}{\partial z} + V(r) \right) \hat{\psi}^{\text{eik.}} = 0. \quad (4.17)$$

The wave function at the eikonal approximation thus reads

$$\psi^{\text{eik.}}(\mathbf{r}) = \exp \left[ ikz - \frac{i}{\hbar v} \int_{-\infty}^z V(\mathbf{b}, z') dz' \right]. \quad (4.18)$$

Coordinate  $\mathbf{r}$  is now written as  $(\mathbf{b}, z)$ . This notation emphasizes the similarity between its transverse part  $\mathbf{b} = (x, y)$  and the semi-classical impact parameter. The asymptotic

expression of the eikonal wave function is however not correct as shown by a comparison with (2.15).

The exact scattering amplitude is formally given by [10, 42, 43]

$$f_k(\Omega) = -\frac{\mu}{2\pi\hbar^2} \int \exp(-i\mathbf{k}' \cdot \mathbf{r}) V(r) \psi(\mathbf{r}) d\mathbf{r}. \quad (4.19)$$

Its calculation requires the resolution of the Schrödinger equation. However this expression is also useful to derive approximations such as the Born expansion. When  $V(r)$  is short-ranged, the correctness of the asymptotics of  $\psi$  is not crucial and (4.19) can be used for deriving a scattering amplitude with the eikonal wave function  $\psi^{\text{eik}}$ .

Let us define the transferred momentum  $\mathbf{q} = \mathbf{k}' - \mathbf{k}$ . At small scattering angles  $\theta$ , the expression  $\mathbf{k}' \cdot \mathbf{r} - kz = \mathbf{q} \cdot \mathbf{r}$  appearing in  $f_k$  can be approximated by  $\mathbf{q} \cdot \mathbf{b}$ . This corresponds to considering  $\mathbf{q}$  as orthogonal to the  $z$  axis. Then the scattering amplitude becomes

$$\begin{aligned} f_k(\theta) &\approx -\frac{\mu}{2\pi\hbar^2} \int d\mathbf{b} e^{-i\mathbf{q} \cdot \mathbf{b}} \int_{-\infty}^{+\infty} dz V(\mathbf{b}, z) \exp\left[-\frac{i}{\hbar v} \int_{-\infty}^z V(\mathbf{b}, z') dz'\right] \\ &= \frac{ik}{2\pi} \int d\mathbf{b} e^{-i\mathbf{q} \cdot \mathbf{b}} [1 - e^{i\chi(\mathbf{b})}] \end{aligned} \quad (4.20)$$

where the phase-shift function is defined as

$$\chi(\mathbf{b}) = -\frac{1}{\hbar v} \int_{-\infty}^{+\infty} V(\mathbf{b}, z) dz. \quad (4.21)$$

Since potential  $V$  is spherically symmetric, one can integrate over  $\varphi$  in (4.20) with

$$J_n(z) = \frac{i^{-n}}{2\pi} \int_0^{2\pi} e^{i(z \cos \varphi - n\varphi)} d\varphi \quad (4.22)$$

and obtain the eikonal amplitude

$$f_k^{\text{eik.}}(\theta) = ik \int_0^\infty b db J_0(qb) [1 - e^{i\chi(b)}]. \quad (4.23)$$

### Coulomb scattering

The analytical case of Coulomb scattering illustrates the problems encountered when the potential is not short-ranged. The phase-shift function takes the simple form

$$\chi_C(b) = -\frac{Z_1 Z_2 e^2}{\hbar v} \int_{-\infty}^{+\infty} \frac{1}{\sqrt{b^2 + z^2}} dz \quad (4.24)$$

but, unfortunately, the integral diverges. Following Ref. [46], let us introduce a cut off  $a \gg b$ . The integral from  $-a$  to  $+a$  gives the dominant term

$$\chi_C(b) \approx 2\eta \ln \frac{b}{2a}. \quad (4.25)$$

The scattering amplitude then reads

$$f_C^{\text{eik.}}(\theta) = f_C(\theta) e^{-2i\eta \ln 2ka} \quad (4.26)$$

where

$$f_C(\theta) = -\frac{\eta}{2k \sin^2 \frac{1}{2}\theta} e^{2i(\sigma_0 - \eta \ln \sin \frac{1}{2}\theta)} \quad (4.27)$$

is the exact quantum expression [10, 42, 43]. Both (4.26) and (4.27) lead to the Rutherford cross section (3.7). However, these amplitudes differ by an arbitrary phase.

## Two-body breakup

Now let us consider the breakup of a two-body system [5, 47-49]. In Eq. (2.28), the relative-motion three-body wave function is replaced by

$$\Psi(\mathbf{R}, \mathbf{r}) = e^{iKZ} \hat{\Psi}(\mathbf{R}, \mathbf{r}) \quad (4.28)$$

with  $\mathbf{K} = \mathbf{k}_P - \mathbf{k}_T$  where  $\mathbf{k}_P$  and  $\mathbf{k}_T$  are the projectile and target wavevectors. The initial projectile-target wavenumber  $K$  is related to the total energy  $E_{\text{tot}}$  in the c.m. frame and to the internal energy  $E_0$  of the projectile by

$$E_{\text{tot}} = \frac{\hbar^2 K^2}{2\mu_{PT}} + E_0. \quad (4.29)$$

With the initial velocity  $v = \hbar K / \mu_{PT}$ , the Schrödinger equation becomes

$$\left( \frac{P^2}{2\mu_{PT}} + vP_Z + H_0 + V_{PT}(\mathbf{R}, \mathbf{r}) - E_0 \right) \hat{\Psi}(\mathbf{R}, \mathbf{r}) = 0. \quad (4.30)$$

Like in (4.16), we assume

$$|\Delta_R \hat{\Psi}| \ll K |\nabla_R \hat{\Psi}| \quad (4.31)$$

at large  $K$ . Moreover we also perform the adiabatic approximation consisting in replacing  $H_0$  by  $E_0$ , i.e. we assume that the internal energy of the projectile does not vary much. This approximation is expected to be especially valid for a weakly-bound halo nucleus. With both approximations, the Schrödinger equation becomes

$$\left( -i\hbar v \frac{\partial}{\partial Z} + V_{PT}(\mathbf{R}, \mathbf{r}) \right) \hat{\Psi}_{\text{eik.}}(\mathbf{R}, \mathbf{r}) = 0. \quad (4.32)$$

The solution satisfying the initial condition (4.11) reads

$$\hat{\Psi}_{\text{eik.}}(\mathbf{R}, \mathbf{r}) = \exp \left[ -\frac{i}{\hbar v} \int_{-\infty}^Z V_{PT}(\mathbf{b}, Z', \mathbf{r}) dZ' \right] \phi_0(\mathbf{r}) \quad (4.33)$$

where coordinate  $\mathbf{R}$  is now written as  $(\mathbf{b}, Z)$  with its transverse part  $\mathbf{b} = (X, Y)$ . A reasoning similar to the one developed for potential scattering leads to the elastic amplitude

$$f_k^{\text{eik.}}(\theta) = iK \int d\mathbf{b} e^{-i\mathbf{q} \cdot \mathbf{b}} S_0^{\text{eik.}}(b). \quad (4.34)$$

The transferred momentum reads here  $\mathbf{q} = \mathbf{K}' - \mathbf{K}$  and

$$S_0^{\text{eik.}}(b) = \lim_{Z \rightarrow +\infty} \langle \phi_0(\mathbf{r}) | \hat{\Psi}_{\text{eik.}}(\mathbf{R}, \mathbf{r}) \rangle - 1. \quad (4.35)$$

The limit of the wave function can be written with  $\mathbf{r} = (\mathbf{r}_\perp, z)$  as

$$\lim_{Z \rightarrow +\infty} \hat{\Psi}_{\text{eik.}}(\mathbf{r}, \mathbf{b}, Z) = e^{i\chi(\mathbf{r}_\perp, \mathbf{b})} \phi_0(\mathbf{r}) \quad (4.36)$$

where, from (4.33) and (2.29),

$$\chi(\mathbf{r}_\perp, \mathbf{b}) = \chi_{cT} \left( \left| \mathbf{b} - \frac{m_f}{m_P} \mathbf{r}_\perp \right| \right) + \chi_{fT} \left( \left| \mathbf{b} + \frac{m_c}{m_P} \mathbf{r}_\perp \right| \right) \quad (4.37)$$

and  $\chi_{cT}(b)$  and  $\chi_{fT}(b)$  are given by (4.21) for  $V_{cT}$  and  $V_{fT}$ , respectively.

The eikonal  $T$ -matrix for breakup is given by

$$T_{fi} \approx i\hbar v \int d\mathbf{b} e^{-i\mathbf{q}\cdot\mathbf{b}} S^{\text{eik.}}(\mathbf{k}, \mathbf{b}) \quad (4.38)$$

with

$$S^{\text{eik.}}(\mathbf{k}, \mathbf{b}) = \lim_{Z \rightarrow +\infty} \langle \phi_{\mathbf{k}}^{(-)}(\mathbf{r}) | \hat{\Psi}_{\text{eik.}}(\mathbf{R}, \mathbf{r}) \rangle = \langle \phi_{\mathbf{k}}^{(-)}(\mathbf{r}) | e^{i\chi(\mathbf{r}_\perp, \mathbf{b})} | \phi_0(\mathbf{r}) \rangle. \quad (4.39)$$

It provides the eikonal approximation of the breakup cross section

$$\frac{d\sigma}{d\mathbf{k}d\Omega} = \frac{KK'}{(2\pi)^5} \left| \int d\mathbf{b} e^{-i\mathbf{q}\cdot\mathbf{b}} S^{\text{eik.}}(\mathbf{k}, \mathbf{b}) \right|^2. \quad (4.40)$$

This expression can be evaluated by a direct integration. It is also convenient to expand it in partial waves [47]. This will be described in section 4.3 for a more general case. Expressions (4.46) to (4.49) and (4.51) are also valid here when using (4.36).

The Coulomb divergence problem is also present here. The divergence can be avoided by truncating the integration at some impact parameter such as  $b_{\text{max}} = \hbar v/2|E_0|$  proposed in Ref. [48]. In Fig. 7, this approximation (dashed line) performed with the potential of Ref. [26] is compared for  $^{11}\text{Be}$  breakup with a first-order perturbation calculation as in Fig. 3 (full line). Here the more recent RIKEN data of Ref. [33] are displayed. In Refs. [50, 51], the eikonal wave function (4.33) has been used as final state in various expressions to deduce possible corrections for the eikonal approximation. Such a correction, which is explicitly displayed and applied in Ref. [49], and does not require any truncation leads to the dotted curve in Fig. 7. These results are closer to experiment. The comparison with experiment would require a convolution with the experimental energy resolution which might still improve the agreement [52].

### 4.3 Dynamical eikonal approximation

Dynamical effects in the projectile or between its fragments are not neglected when the eikonal approximation (4.31) is performed but the adiabatic approximation  $H_0 \rightarrow E_0$  is not performed. The Schrödinger equation for the dynamical eikonal approximation (DEA) then reads

$$i\hbar v \frac{\partial}{\partial Z} \hat{\Psi}(\mathbf{R}, \mathbf{r}) = (H_0 + V_{PT} - E_0) \hat{\Psi}(\mathbf{R}, \mathbf{r}). \quad (4.41)$$

With the replacement  $t = Z/v$ , this equation is formally identical to the semi-classical Schrödinger equation (3.1) with straight-line trajectories [53, 54]. The solution  $\hat{\Psi}(\mathbf{R}, \mathbf{r})$  of (4.41) is thus proportional to the solution  $\hat{\Psi}_{\text{s.c.}}(\mathbf{r}, Z/v)$  of the TDSE (3.1). However, some care must be taken here because one needs this solution for all values of vector  $\mathbf{b}$ . The TDSE must be solved for each impact parameter  $b$  but one does not wish to solve

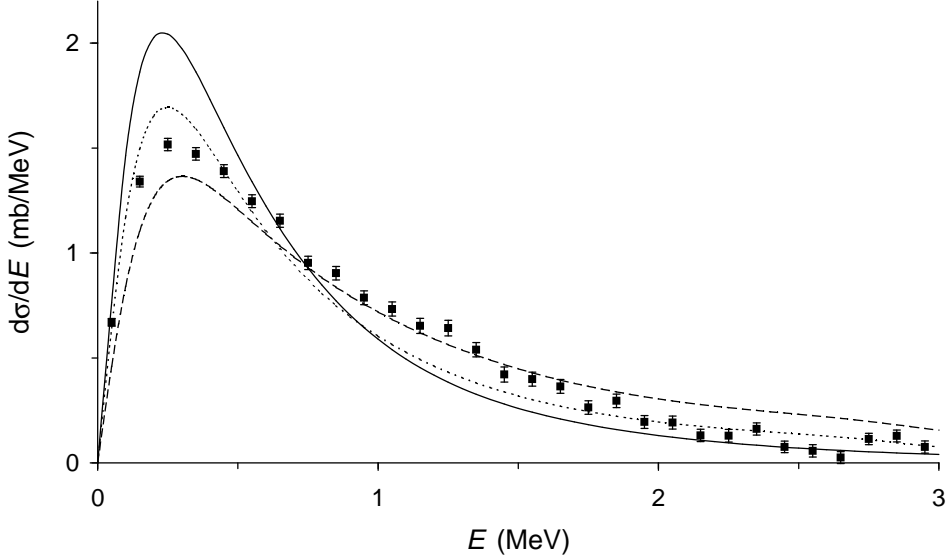


Figure 7: Angle-integrated cross sections for the elastic breakup of  $^{11}\text{Be}$  on  $^{208}\text{Pb}$  at 68 MeV/nucleon. Eikonal approximation with cutoff (dashed line) and with a correction [51, 49] (dotted line). The first-order results (full line) are shown for comparison. Experimental data from  $0^\circ$  to  $6^\circ$  (dots) [33].

it more than once at a given  $b$ . For a given ‘impact parameter’  $b$ , solutions at different angles (see Fig. 8) are coherently related by a rotation as [54]

$$\Psi_{\text{DEA}}(\mathbf{R}, \mathbf{r}) = e^{iKZ} e^{-i\varphi_b l_z} \hat{\Psi}_{\text{s.c.}}(\mathbf{r}, Z/v). \quad (4.42)$$

The elastic-breakup amplitude can be defined as

$$S(\mathbf{k}, \mathbf{b}) = \lim_{Z \rightarrow +\infty} \langle \phi_{\mathbf{k}}^{(-)}(\mathbf{r}) | \hat{\Psi}_{\text{s.c.}}(\mathbf{r}, Z/v) \rangle \quad (4.43)$$

and provides the breakup cross section (4.40) but now for the DEA. It is more convenient to use a partial-wave expansion

$$S(\mathbf{k}, \mathbf{b}) = (2\pi)^{3/2} k^{-1} \sum_{lm} Y_l^m(\Omega_k) e^{-im\varphi_b} S_{klm}(b). \quad (4.44)$$

If the semi-classical cross section is expanded as

$$\lim_{Z \rightarrow +\infty} \hat{\Psi}_{\text{s.c.}}(\mathbf{r}, Z/v) = \frac{1}{r} \sum_{lm} \hat{\psi}_{lm}(r) Y_l^m(\Omega_r), \quad (4.45)$$

the partial breakup amplitudes are simply given by

$$S_{klm}(b) = \lim_{Z \rightarrow +\infty} \langle \phi_{klm}^{(-)} | \hat{\Psi}_{\text{s.c.}}(\mathbf{r}, Z/v) \rangle = i^{-l} e^{i(\sigma_l + \delta_l)} \int_0^\infty u_{kl}(r) \hat{\psi}_{lm}(r) dr. \quad (4.46)$$

With (4.22), the cross section reads

$$\frac{d\sigma}{dkd\Omega} = \frac{KK'}{k^2} \left| \sum_{lm} i^{-|m|} Y_l^m(\Omega_k) e^{-im\varphi} \int_0^\infty b db J_{|m|}(qb) S_{klm}(b) \right|^2. \quad (4.47)$$

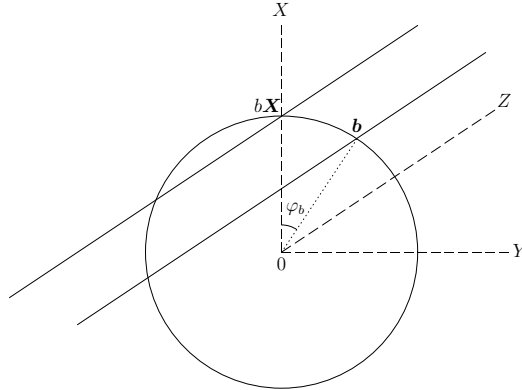


Figure 8: Schematic representation of the rotation in Eq. (4.42) between trajectories parallel to the  $Z$  axis (full lines) with impact vectors  $b\mathbf{X}$  at angle 0 and  $\mathbf{b}$  at angle  $\varphi_b$ .

It depends on the angle difference  $\varphi_k - \varphi$  of the azimuthal angles of  $\mathbf{k}$  and  $\mathbf{K}'$  and is thus invariant with respect to rotations around the  $Z$  axis.

When the direction of emission of the fragments is not determined, an integration over  $\Omega_k$  and a change of variable lead to

$$\frac{d\sigma}{dE d\Omega} = \frac{KK'}{\hbar v_{cf}} \sum_{lm} \left| \int_0^\infty b db J_{|m|}(qb) S_{klm}(b) \right|^2. \quad (4.48)$$

When the projectile c.m. direction is not determined, an integration over  $\Omega$  with  $q = 2K \sin \frac{1}{2}\theta$  and  $KK' \approx K^2$  provides

$$\frac{d\sigma}{dE} = \frac{2\pi}{\hbar v_{cf}} \sum_{lm} \int_0^\infty b db S_{klm}^*(b) \int_0^\infty b' db' S_{klm}(b') \int_0^{2K} q dq J_{|m|}(qb) J_{|m|}(qb'). \quad (4.49)$$

Since wavenumber  $K$  is large, one can approximate the upper bound of the integral over  $q$  by  $+\infty$ . The resulting integral is

$$\int_0^\infty q dq J_m(qb) J_m(qb') = \frac{1}{b} \delta(b - b') \quad (4.50)$$

and leads to the expression

$$\frac{d\sigma}{dE} \approx \frac{2\pi}{\hbar v_{cf}} \sum_{lm} \int_0^\infty b db |S_{klm}(b)|^2 \quad (4.51)$$

which is identical to the semi-classical expression (3.14). Notice that Coulomb effects do not cause any divergence in the DEA.

The DEA has the important advantage over a semi-classical calculation that it provides elastic differential cross sections. In the left panel of Fig. 9, the elastic scattering of  $^{11}\text{Be}$  on  $^{12}\text{C}$  [53] is compared with GANIL data at 49.3 MeV/nucleon [55]. The agreement is very good. However, the simpler eikonal approximation (4.34) provides a similar agreement. In the right panel, the results of both approximations are compared for the elastic scattering of  $^{11}\text{Be}$  on the heavier target  $^{208}\text{Pb}$  at the lower energy

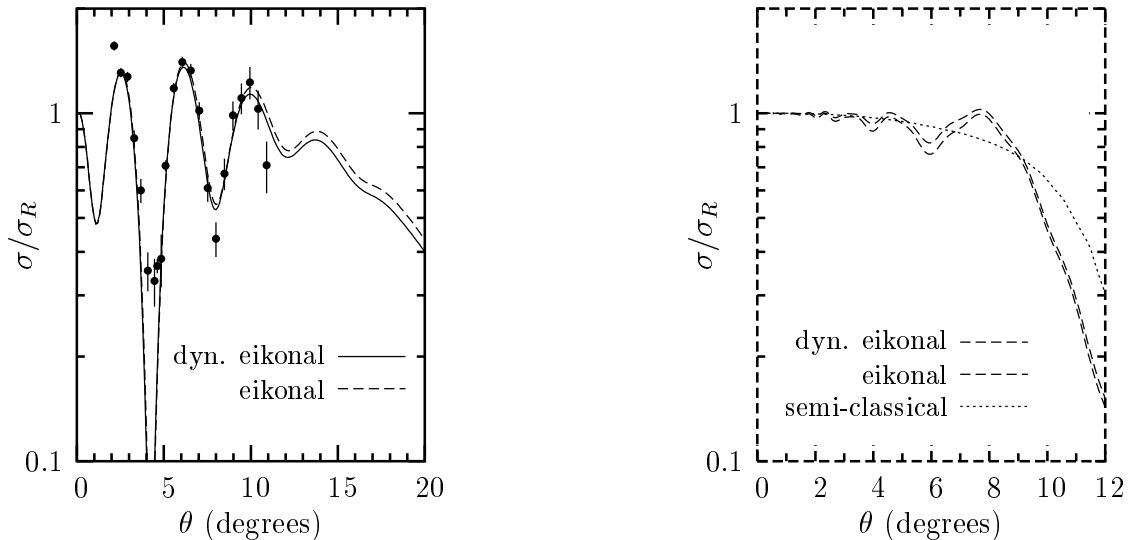


Figure 9: Elastic scattering of  $^{11}\text{Be}$  on  $^{12}\text{C}$  at 49.3 MeV/nucleon (left) and on  $^{208}\text{Pb}$  at 20 MeV/nucleon (right) (Figs. 1 and 2 from Ref. [53]). Experimental data from Ref. [55].

20 MeV/nucleon. Because Coulomb breakup dominates, the difference between both approximations is larger but they remain qualitatively similar. A semi-classical cross section (dotted line) can be calculated here with a Coulomb trajectory. The average behaviour of the differential cross section is reproduced but interference effects are missing.

Angle-integrated breakup cross sections of  $^{11}\text{Be}$  on  $^{208}\text{Pb}$  at 69 MeV/nucleon are displayed in Fig. 10 [54]. One observes that approximation (4.51), or equivalently a semi-classical calculation, give very close results to those of an angular integration from 0 to 6 degrees. They slightly underestimate the experimental data [33]. An integration up to  $1.3^\circ$  corresponding to large impact parameters is in an even better agreement with the data except possibly beyond 1 MeV. It indicates that the spectroscopic factor should be close to one.

The breakup of  $^8\text{B}$  on  $^{208}\text{Pb}$  is illustrated in Figs. 11 and 12. Here the fragment is a proton. The E2 effective charge is much larger (see section 3.4). Several experiments have attempted to evaluate the importance of the E2 contribution. Longitudinal momentum distributions of  $^7\text{Be}$  are especially sensitive to the interference between the E1 and E2 multipoles. Such an effect induces an asymmetry in the data of Ref. [56]. This asymmetry is obtained with first-order perturbation theory but could not be reproduced in CDCC calculations [57] (see Fig. 14). One observes in Fig. 11 that the E2 component is essential to induce this asymmetry. Without any adjusted parameter, the DEA provides a fair reproduction of data at 44 MeV/nucleon but the agreement is not so good at 81 MeV/nucleon [58]. Angular distributions measured at RIKEN [59] are also well reproduced by the DEA under exactly the same conditions of calculation. If valid, first-order perturbation theory would allow extracting the radiative-capture cross section (3.30) from breakup data but the E2 component and the role of higher-order corrections make this extraction difficult and thus inaccurate [58].

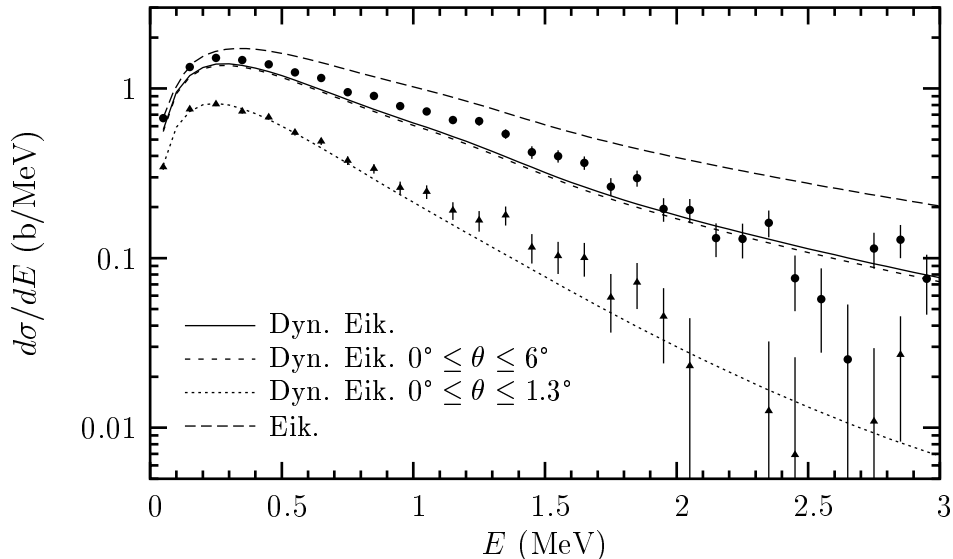


Figure 10: Angle-integrated cross sections for the elastic breakup of  $^{11}\text{Be}$  on  $^{208}\text{Pb}$  at 69 MeV/nucleon (Fig. 9 from Ref. [54]). The curve labeled 'Dyn. Eik.' is obtained with Eq. (4.51). The curve labeled 'Eik.' corresponds to the eikonal approximation (4.39). The other curves are obtained by integrating numerically Eq. (4.47). Experimental data from  $0^\circ$  to  $6^\circ$  (dots) and from  $0^\circ$  to  $1.3^\circ$  (triangles) [33].

#### 4.4 Method of coupled discretized-continuum channels

The principle of a coupled-channel method is to expand the wave function in Eq. (2.28) over the complete set of eigenstates of  $H_0$ , the coefficients of the expansion depending on  $\mathbf{R}$ . The unknown coefficients satisfy an infinite system of coupled differential equations which must be truncated at some level. When there is only one bound state, this procedure becomes much more complicated because of the important role played by continuum states.

The expansion can in principle be performed over stationary scattering states as [60, 61]

$$\Psi(\mathbf{R}, \mathbf{r}) = \phi_0(\mathbf{r})X_0(\mathbf{R}) + \int \phi_{\mathbf{k}}^{(+)}(\mathbf{r})X_{\mathbf{k}}(\mathbf{R})d\mathbf{k}. \quad (4.52)$$

This procedure is not usable in practice. First, one has to take rotational invariance into account and expand the partial wave for each total angular momentum  $J$ . Indeed the three-body Hamiltonian commutes with the total orbital momentum  $\mathbf{J} = \mathbf{l} + \mathbf{L}$  [Eq. (2.27)]. The existence of the good quantum numbers  $J$  and  $M$  leads to a simpler partial-wave expansion

$$\Psi^{JM}(\mathbf{R}, \mathbf{r}) = (rR)^{-1} \left( \sum_L Y_{l_0 L}^{JM} u_{0l_0}(r) X_{0l_0 L}^J(R) + \sum_{lL} Y_{lL}^{JM} \int_0^\infty u_{kl}(r) X_{klL}^J(R) dk \right) \quad (4.53)$$

where  $u_{0l_0}$  is the ground-state radial wave function and  $u_{kl}$  is defined by (2.10) and (2.11). The coupled spherical harmonics

$$Y_{lL}^{JM}(\Omega_r, \Omega_R) = \sum_{mm'} (lLmm'|JM) Y_l^m(\Omega_r) Y_L^{m'}(\Omega_R) \quad (4.54)$$

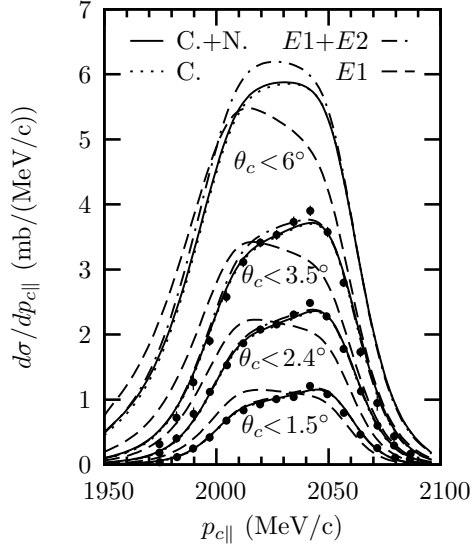


Figure 11: DEA calculations of longitudinal momentum distributions of  ${}^7\text{Be}$  obtained by dissociation of  ${}^8\text{B}$  on Pb at 44 MeV/nucleon for various  ${}^7\text{Be}$  scattering-angle cuts (Fig. 1 from Ref. [58]). Experimental data from [56]. DEA calculations are performed using Coulomb plus nuclear (full lines), purely Coulomb (dotted lines),  $E1 + E2$  (dash-dotted lines), and  $E1$  (dashed lines)  $P$ - $T$  interactions.

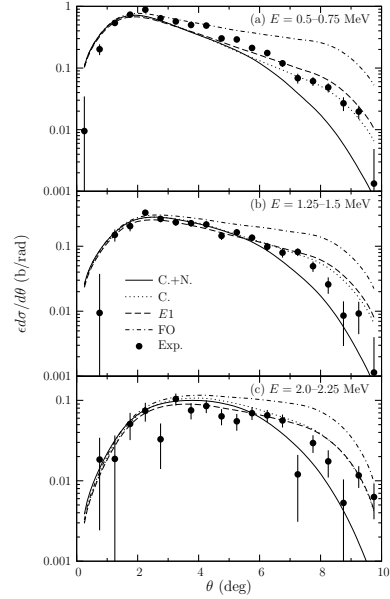


Figure 12: DEA calculations of angular distributions for the breakup of  ${}^8\text{B}$  on Pb at 52 MeV/nucleon over three energy ranges: DEA calculations (with convolution) using Coulomb plus nuclear (full lines), purely Coulomb (dotted lines), and  $E1$  (dashed lines)  $P$ - $T$  interactions; first-order calculations with  $E1 + E2$  strengths (dash-dotted lines) (Fig. 6 from Ref. [58]). Experimental data from [59].

are common eigenfunctions of  $\mathbf{l}^2$ ,  $\mathbf{L}^2$ ,  $\mathbf{J}^2$  and  $J_z$ . Since  $l$  and  $L$  are not good quantum numbers, they appear as summation indices in (4.53). The corresponding system would also involve a continuous infinity of equations because the expansion in scattering functions  $\phi_{klm}$  still contains an integral over wavenumber  $k$ .

Therefore, it has been proposed to replace  $\phi_{klm}$  by a discretized continuum [60], i.e. by a finite set of square-integrable functions

$$\phi_{klm} \rightarrow \phi_{ilm} = r^{-1}u_{il}(r)Y_l^m(\Omega_r), \quad i = 1, \dots, N \quad (4.55)$$

satisfying for each partial wave the orthonormality conditions

$$\langle \phi_{ilm} | \phi_{i'lm} \rangle = \delta_{ii'} \quad (4.56)$$

and diagonalizing the internal Hamiltonian

$$\langle \phi_{ilm} | H_0 | \phi_{i'lm} \rangle = E_{il} \delta_{ii'}. \quad (4.57)$$

The discrete energies  $E_{il}$  are positive, except the ground-state energy  $E_{0l_0} < 0$ . They have no physical meaning unless they correspond to some narrow resonance.

The method of coupled discretized-continuum channels [60, 61, 62] (or continuum-discretized coupled channels [63]) is better known as CDCC. The CDCC approximation consists in the finite expansion [45, 57, 60-69]

$$\Psi_{\text{CDCC}}^{JM}(\mathbf{R}, \mathbf{r}) = (rR)^{-1} \sum_{i=1}^N \sum_{lL} Y_{iL}^{JM} u_{il}(r) X_{iL}^J(R). \quad (4.58)$$

The sum includes the bound state and the discretized scattering states. Introducing (4.58) in the Schrödinger equation (2.28) and projecting leads to the  $N$  coupled-channel equations

$$\left[ -\frac{\hbar^2}{2\mu_{PT}} \left( \frac{d^2}{dR^2} - \frac{L(L+1)}{R^2} \right) + V_{iL, iL}^J(R) + E_{il} - E_{\text{tot}} \right] X_{iL}^J(R) + \sum_{i' L' \neq iL} V_{iL, i' L'}^J(R) X_{i' L'}^J(R) = 0. \quad (4.59)$$

The potential matrix elements are defined by

$$V_{iL, i' L'}^J(R) = \langle Y_{iL}^{JM} r^{-1} u_{il} | V_{PT} | Y_{i' L'}^{JM} r^{-1} u_{i' l'} \rangle. \quad (4.60)$$

In this expression, the integration is performed over  $\mathbf{r}$  and  $\Omega_R$ . Equations (4.59) can now be solved in analogy with those of the traditional coupled-channel problem [70].

Two main variants exist for the choice of the discretized continuum. In the first variant, pseudostates are constructed by solving the Schrödinger equation for the internal motion using the expansion [61, 62, 65, 69]

$$\phi_{ilm}(\mathbf{r}) = \sum_{j=1}^N C_{jl}^{(i)} \varphi_{jlm}(\mathbf{r}) \quad (4.61)$$

where some square-integrable basis states have been chosen as

$$\varphi_{jlm}(\mathbf{r}) = \Gamma_{jl}(r) Y_l^m(\Omega_r). \quad (4.62)$$

The  $\Gamma_{jl}$  are often Gaussian functions [62, 63] or can be based on a transformed harmonic oscillator [69]. The energies and coefficients are given by the system of  $N$  variational equations

$$\sum_{j=1}^N (\langle \varphi_{j'lm} | H_0 | \varphi_{jlm} \rangle - E_{il} \langle \varphi_{j'lm} | \varphi_{jlm} \rangle) C_{jl}^{(i)} = 0. \quad (4.63)$$

Usually, only states below some chosen maximal energy are kept in the CDCC calculation.

The second variant consists in constructing average scattering states over momentum bins [60, 62, 66],

$$\phi_{ilm}(\mathbf{r}) = \frac{1}{W_i} \int_{k_{i-1}}^{k_i} \phi_{klm}(\mathbf{r}) f_i(k) dk. \quad (4.64)$$

Such states are square-integrable if  $f_i$  is square-integrable. They are orthogonal because of (2.7). They are normed when

$$W_i = \left( \int_{k_{i-1}}^{k_i} |f_i(k)|^2 dk \right)^{1/2}. \quad (4.65)$$

The energies are given by

$$E_{il} = \frac{\hbar^2}{2\mu_{cf}W_i^2} \int_{k_{i-1}}^{k_i} |f_i(k)|^2 k^2 dk. \quad (4.66)$$

A simple example for non-resonant states is given by  $f_i(k) = 1$  and  $W_i = (k_i - k_{i-1})^{1/2}$ . The corresponding energies are

$$E_{il} = \frac{\hbar^2(k_i^2 + k_i k_{i-1} + k_{i-1}^2)}{6\mu_{cf}}. \quad (4.67)$$

Basis states with  $f_i(k) = 1$  are mostly used for  $l > 0$  [45]. For a resonance, a discretization in small momentum bins requires too much computer time. The Lorentzian form factor  $f_{il}(k) = i\frac{1}{2}\Gamma/(E - E_{Rl} + i\frac{1}{2}\Gamma)$  is preferable [71, 63]. The average energy is then equal to the resonance energy  $E_{il} = E_{Rl}$ .

In order to calculate the cross section (4.12), one needs an expression for the partial transition matrix element

$$T_{iL}^J(K, k) = \langle Y_{iL}^{JM} R^{-1} u_{KL}^{(-)}(R) r^{-1} u_{kl}^{(-)}(r) | V_{PT} | \Psi_{CDCC}^{JM}(\mathbf{R}, \mathbf{r}) \rangle \quad (4.68)$$

where the wave function is replaced by its CDCC approximation. The  $u^{(-)}$  radial functions are defined by (2.23) but here for plane or Coulomb waves. However, what is available is the discretized expression

$$\hat{T}_{jL}^J(K) = \langle Y_{iL}^{JM} R^{-1} u_{KL}^{(-)}(R) r^{-1} u_{jl}(r) | V_{PT} | \Psi_{CDCC}^{JM}(\mathbf{R}, \mathbf{r}) \rangle. \quad (4.69)$$

Its calculation requires a multipole expansion of the interaction. The situation is schematically depicted in Fig 13. An approximation of (4.68) can be obtained by interpolation. Using in (4.68) the approximate closure relation

$$\sum_{jlm} |\phi_{jlm}\rangle \langle \phi_{jlm}| \approx 1, \quad (4.70)$$

one obtains from (4.69) [45]

$$T_{iL}^J(K, k) \approx \sum_j \langle \phi_{klm}^{(-)} | \phi_{jlm} \rangle \hat{T}_{jL}^J(K). \quad (4.71)$$

This expression can be used with both types of discretized continuum.

The results of CDCC calculations for the  $^8\text{B}$  breakup into  $^7\text{Be}$  and  $p$  are displayed in Figs. 14 and 15. Fig. 14 should be compared with Fig. 11 since both models concern the same experimental data [56]. The CDCC results do not reproduce the asymmetry of the data (left panel) [57]. Increasing the E2 component by a factor 1.6 leads to a good agreement with experiment (right panel) but this modification can not receive a physical justification.

In Fig. 15 are displayed CDCC results [68] corresponding to the upper panel in Fig. 12. Cross sections are presented with (filtered) and without (unfiltered) convolution with the experimental energy resolution. The quality of the agreement with experiment is similar for CDCC and for DEA, which indicates that both methods are accurate in this projectile-energy domain.

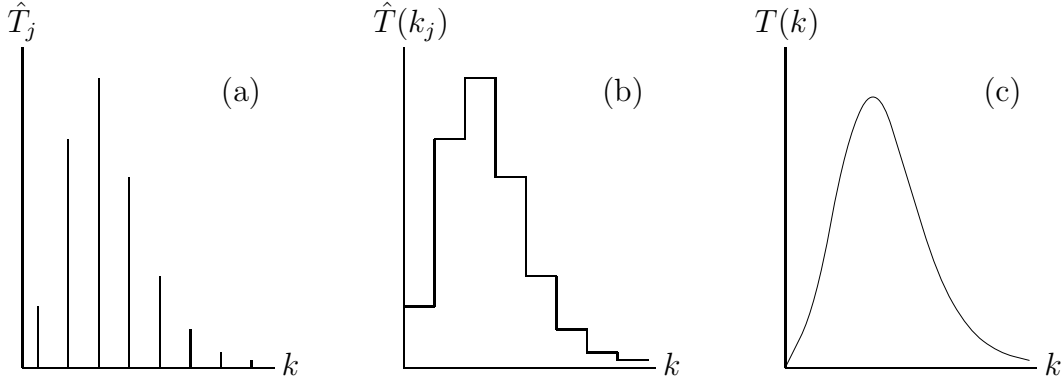


Figure 13: Schematic representation of the different types of approximation (adapted from Ref. [63]): (a) Eq. (4.69) for pseudostates, (b) Eq. (4.69) for momentum bins, (c) interpolation (4.71).

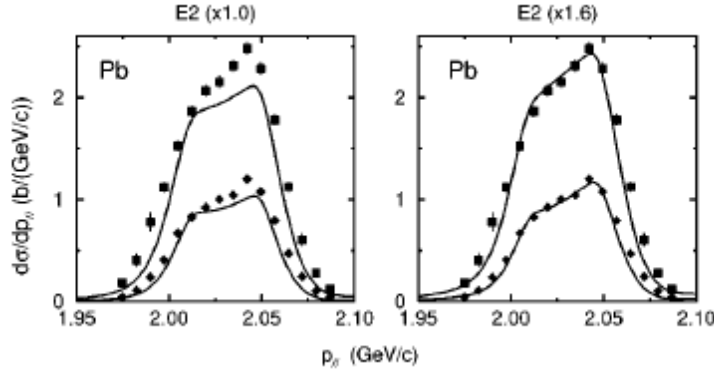


Figure 14: CDCC calculations of longitudinal momentum distributions of  ${}^7\text{Be}$  obtained by dissociation of  ${}^8\text{B}$  on Pb at 44 MeV/nucleon for  ${}^7\text{Be}$  scattering angles smaller than 2.4 and 1.5 degrees (Fig. 5 from Ref. [57]). Experimental data from [56].

## 4.5 Summary and comments

The CDCC method, as a purely quantal method, has the advantage of being valid at low energies but can also be applied at rather high energies. Besides its long computational times, its main drawback is the difficulty of assessing its convergence. The discretization of the continuum requires some skill. Controlling the accuracy is difficult. Extensions to core excitation are in progress [72]. Among the two different types of bases used, the pseudostate basis seems more promising for studying the breakup of three-body projectiles [73].

The dynamical eikonal approximation is only valid at rather high energies and rather small scattering angles. Coulomb effects are treated without difficulty. The DEA improves and complements the semi-classical approximation for which various codes are available. An extension to three-body projectiles is difficult as it involves much larger computing times.

The usual eikonal approximation is significantly simpler but needs care when dealing

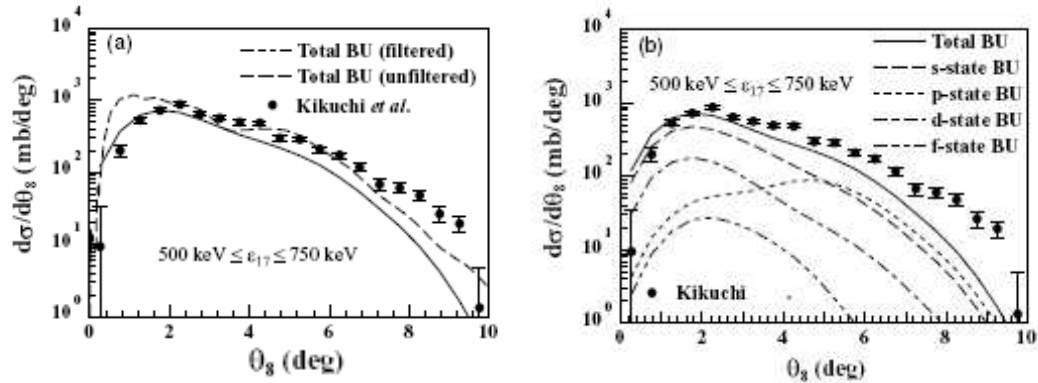


Figure 15: CDCC angular distributions for the breakup of  ${}^8\text{B}$  on Pb at 52 MeV/nucleon over the 0.5 – 0.75 energy range (Fig. 3 from Ref. [68]). Left panel: influence of convolution (filtering); right panel: partial-wave decomposition. Experimental data from [59].

with the Coulomb force. The error introduced by Coulomb terms can not easily be estimated. It provides physically good results when the nuclear force dominates.

Other methods exist such as the adiabatic approximation [74, 75] or DWBA [76, 77].

## 5 Conclusion

The theory of breakup reactions offers several accurate approximations covering a broad energy range that allow an interpretation of various experiments. However, it is based until now on rather simple, and even too simple, models of the projectile structure. The sensitivity to the projectile model seems to be rather weak provided that the value of the projectile binding energy is correct. The precise form of final scattering states is often assumed not to play a significant role but this point deserves verification.

An additional difficulty is that experiments are not very accurate and usually require unpleasant convolutions of theoretical results to simulate the resolution and acceptance of the detectors. Little can then be learned about the projectile from two-body breakup reactions. The determination of spectroscopic factors is affected by various uncertainties (accuracy of the normalization of the data, knowledge of ANC, choice of potential). The two-body breakup on a light target can be used as a tool to search for resonances. The Coulomb breakup on heavy targets is useful for assessing astrophysical  $S$  factors for nuclear astrophysics but its accuracy is uncertain [58].

Several methods can now be applied to three-body breakup (CDCC, eikonal, ...). They will allow studying coincidence observables that are more difficult to measure but less sensitive to the absolute normalization of cross sections. They should lead to interesting information about the projectile structure through the study of correlations between the emitted fragments.

The main challenge for models is to improve the projectile description by using microscopic models, involving nucleon-nucleon forces and full antisymmetrization. Before

such calculations can be performed with ab initio wave functions [78], a useful step will be extending the present reaction models to projectile descriptions within the simpler microscopic cluster model [79].

## Acknowledgments

I thank V. Melezhik, P. Capel and G. Goldstein for our fruitful collaborations. I also thank Y. Suzuki for interesting discussions on the eikonal approximation. This text presents research results of the Belgian program P5/07 on interuniversity attraction poles initiated by the Belgian-state Federal Services for Scientific, Technical and Cultural Affairs.

## Appendix A: Hyperbolic trajectory

Parametric equations of an hyperbolic Coulomb (or Rutherford) trajectory are given by [14]

$$R = a(\epsilon \cosh \omega + 1), \quad (\text{A.1})$$

$$\cos \vartheta = \frac{\sqrt{\epsilon^2 - 1} \sinh \omega}{\epsilon \cosh \omega + 1}, \quad (\text{A.2})$$

$$vt = a(\epsilon \sinh \omega + \omega), \quad (\text{A.3})$$

as a function of a parameter  $\omega$  varying from  $-\infty$  to  $+\infty$ . In (A.2),  $\vartheta$  is the angle between  $\mathbf{R}$  and the symmetry axis of the trajectory. As a function of the scattering angle  $\theta$ , the eccentricity parameter  $\epsilon$  is defined by

$$\epsilon = \frac{1}{\sin \frac{1}{2}\theta} \quad (\text{A.4})$$

and the impact parameter  $b$  is given by

$$b = a \cot \frac{1}{2}\theta. \quad (\text{A.5})$$

In these expressions,  $a = Z_P Z_T e^2 / 2E$  is half the distance of closest approach in head-on collisions.

# Bibliography

- [1] I. Tanihata, J. Phys. G **22**, (1996) 157.
- [2] P.G. Hansen, A.S. Jensen and B. Jonson, Annu. Rev. Nucl. Part. Sci. **45**, (1995) 505.
- [3] T. Aumann, Eur. Phys. J. A **26**, (2005) 441.
- [4] M.D. Cortina-Gil, *Réactions de dissociation: aspects expérimentaux*, Ecole Joliot-Curie, Maubuisson 2007.
- [5] K. Hencken, G.F. Bertsch and H. Esbensen, Phys. Rev. C **54**, (1996) 3043.
- [6] G. Baur, C.A. Bertulani and H. Rebel, Nucl. Phys. **A458**, (1986) 188.
- [7] G. Baur, K. Hencken and D. Trautmann, Prog. Part. Nucl. Phys. **51**, (2003) 487.
- [8] J. Al-Khalili and F. Nunes, J. Phys. G **29**, (2003) R89.
- [9] D. Baye, Proceedings Les Houches 2007, to be published.
- [10] C.J. Joachain, *Quantum Collision Theory* (North-Holland, Amsterdam, 1975).
- [11] M. Abramowitz and I.A. Stegun, *Handbook of Mathematical Functions* (Dover, New York, 1970).
- [12] P.E. Hodgson, *Nuclear heavy-ion reactions* (Clarendon, Oxford, 1978).
- [13] Y. Suzuki, R.G. Lovas, K. Yabana and K. Varga, *Structure and reactions of light exotic nuclei* (Taylor and Francis, London, 2003).
- [14] K. Alder and A. Winther, *Electromagnetic excitation* (North-Holland, Amsterdam, 1975).
- [15] G.F. Bertsch and C.A. Bertulani, Nucl. Phys. **A556**, (1993) 136.
- [16] C.A. Bertulani and G.F. Bertsch, Phys. Rev. C **49**, (1994) 2839.
- [17] T. Kido, K. Yabana and Y. Suzuki, Phys. Rev. C **50**, (1994) R1276.
- [18] H. Esbensen, G.F. Bertsch and C.A. Bertulani, Nucl. Phys. **A581**, (1995) 107.
- [19] H. Esbensen and G.F. Bertsch, Nucl. Phys. **A600**, (1996) 37.
- [20] T. Kido, K. Yabana and Y. Suzuki, Phys. Rev. C **53**, (1996) 2296.

- [21] S. Typel and H.H. Wolter, Z. Naturforsch. A **54**, (1999) 63.
- [22] V.S. Melezhik and D. Baye, Phys. Rev. C **59**, (1999) 3232.
- [23] V.S. Melezhik and D. Baye, Phys. Rev. C **64**, (2001) 054612.
- [24] S. Typel and R. Shyam, Phys. Rev. C **64**, (2001) 024605.
- [25] M. Fallot, J.A. Scarpaci, D. Lacroix, P. Chomaz and J. Margueron, Nucl. Phys. **A700**, (2002) 70.
- [26] P. Capel, D. Baye and V.S. Melezhik, Phys. Rev. C **68**, (2003) 014612.
- [27] H. Esbensen and C.A. Bertulani, Phys. Rev. C **65**, (2002) 024605.
- [28] C. Angulo, M. Arnould, M. Rayet, P. Descouvemont, D. Baye, C. Leclercq-Willain, A. Coc, S. Barhoumi, P. Aguer, C. Rolfs et al., Nucl. Phys. **A656**, (1999) 3.
- [29] D. Baye and E. Brainis, Phys. Rev. C **61**, (2000) 025801.
- [30] P. Capel and D. Baye, Phys. Rev. C **71**, (2005) 044609.
- [31] S. Typel and G. Baur, Nucl. Phys. **A759** (2005) 247.
- [32] T. Nakamura, S. Shimoura, T. Kobayashi, T. Teranishi, K. Abe, N. Aoi, Y. Doki, M. Fujimaki, N. Inabe, N. Iwasa et al., Phys. Lett. B **331**, (1994) 296.
- [33] N. Fukuda, T. Nakamura, N. Aoi, N. Imai, M. Ishihara, T. Kobayashi, H. Iwasaki, T. Kubo, A. Mengoni, M. Notani et al., Phys. Rev. C **70**, (2004) 054606.
- [34] P. Capel and F.M. Nunes, Phys. Rev. C **73**, (2006) 014615.
- [35] R. Palit, P. Adrich, T. Aumann, K. Boretzky, B.V. Carlson, D. Cortina, U. Datta Pramanik, T.W. Elze, H. Emling, H. Geissel et al., Phys. Rev. C **68**, (2003) 034318.
- [36] T. Nakamura, N. Fukuda, N. Aoi, H. Iwasaki, T. Kobayashi, T. Kubo, A. Mengoni, M. Notani, H. Otsu, H. Sakurai et al., Nucl. Phys. **A722**, (2003) 301c.
- [37] P. Capel, G. Goldstein and D. Baye, Phys. Rev. C **70**, (2004) 064605.
- [38] S. Typel and G. Baur, Phys. Rev. C **64**, (2001) 024601.
- [39] H. Esbensen and G.F. Bertsch, Nucl. Phys. **A706**, (2002) 383.
- [40] H. Esbensen, G.F. Bertsch and K.A. Snover, Phys. Rev. Lett. **94**, (2005) 042502.
- [41] D. Baye, *Reaction mechanisms for rare isotope beams*, Editor B.A. Brown, AIP Conf. Proc. **791** (AIP, New York, 2005) p. 1.
- [42] M.L. Goldberger and K.M. Watson, *Collision Theory*, (John Wiley & Sons, New York, 1964).

- [43] R.G. Newton, *Scattering Theory of Waves and Particles* (Springer, New York, 1982).
- [44] H. Fuchs, Nucl. Instrum. Meth. **200**, (1982) 361.
- [45] J.A. Tostevin, F.M. Nunes and I.J. Thompson, Phys. Rev. C **63**, (2001) 024617.
- [46] R.J. Glauber, *High energy collision theory* in Lectures in Theoretical Physics, Vol. 1, Editors W.E. Brittin and L.G. Dunham (Interscience, New York, 1959) p. 315.
- [47] H. Esbensen and G.F. Bertsch, Phys. Rev. C **64**, (2001) 014608.
- [48] B. Abu-Ibrahim and Y. Suzuki, Phys. Rev. C **62**, (2000) 034608.
- [49] B. Abu-Ibrahim and Y. Suzuki, Prog. Theor. Phys. **112**, (2004) 1013.
- [50] J. Margueron, A. Bonaccorso and D.M. Brink, Nucl. Phys. **A703**, (2002) 105.
- [51] J. Margueron, A. Bonaccorso and D.M. Brink, Nucl. Phys. **A720**, (2003) 337.
- [52] B. Abu-Ibrahim and Y. Suzuki, Prog. Theor. Phys. **114**, (2005) 901.
- [53] D. Baye, P. Capel and G. Goldstein, Phys. Rev. Lett. **95**, (2005) 082502.
- [54] G. Goldstein, D. Baye and P. Capel, Phys. Rev. C **73**, (2006) 024602.
- [55] M.D. Cortina-Gil, PhD thesis, Université de Caen (1996).
- [56] B. Davids, D.W. Anthony, S.M. Austin, D. Bazin, B. Blank, J. Caggiano, M. Chartier, H. Esbensen, P. Hui, C. Powell et al., Phys. Rev. Lett. **81**, (1998) 2209.
- [57] J. Mortimer, I. J. Thompson and J. A. Tostevin, Phys. Rev. C **65**, (2002) 064619.
- [58] G. Goldstein, P. Capel and D. Baye, Phys. Rev. C **76**, (2007) 024608.
- [59] T. Kikuchi, T. Motobayashi, N. Iwasa, Y. Ando, M. Kurokawa, S. Moriya, H. Murakami, T. Nishio, J. Ruan (Gen), S. Shirato et al., Phys. Lett. B **391**, (1997) 261.
- [60] G. Rawitscher, Phys. Rev. C **9**, (1974) 2210.
- [61] R.Y. Rasoanaivo and G. Rawitscher, Phys. Rev. C **39**, (1989) 1709.
- [62] M. Kawai, Prog. Theor. Phys. Suppl. **89**, (1986) 11.
- [63] T. Matsumoto, T. Kamizato, K. Ogata, Y. Iseri, E. Hiyama, M. Kamimura and M. Yahiro, Phys. Rev. C **68**, (2003) 064607.
- [64] M. Yahiro, Y. Iseri, H. Kameyama, M. Kamimura and M. Kawai, Prog. Theor. Phys. Suppl. **89**, (1986) 22.

- [65] N. Austern, Y. Iseri, M. Kamimura, M. Kawai, G. Rawitscher and M. Yahiro, Phys. Rep. **154**, (1987) 125.
- [66] F.M. Nunes and I. J. Thompson, Phys. Rev. C **59**, (1999) 2652.
- [67] K. Ogata, M. Yahiro, Y. Iseri, T. Matsumoto and M. Kamimura, Phys. Rev. C **68**, (2003) 064609.
- [68] K. Ogata, S. Hashimoto, Y. Iseri, M. Kamimura and M. Yahiro, Phys. Rev. C **73**, (2006) 024605.
- [69] A.M. Moro, F. Pérez-Bernal, J.M. Arias and J. Gómez-Camacho, Phys. Rev. C **73**, (2006) 044612.
- [70] P. Fröbrich and R. Lipperheide, *Theory of Nuclear Reactions* (Clarendon, Oxford, 1996).
- [71] Y. Sakuragi, M. Yahiro and M. Kamimura, Prog. Theor. Phys. Suppl. **89**, (1986) 136.
- [72] N.C. Summers, F.M. Nunes and I. J. Thompson, Phys. Rev. C **74**, (2006) 014606.
- [73] T. Matsumoto, T. Ogami, K. Ogata, Y. Iseri, M. Kamimura and M. Yahiro, Phys. Rev. C **73**, (2006) 051602.
- [74] R.C. Johnson, J.S. Al-Khalili and J.A. Tostevin, Phys. Rev. Lett. **79**, (1997) 2771.
- [75] J.A. Tostevin, S. Rugmai and R.C. Johnson, Phys. Rev. C **57**, (1998) 3225.
- [76] R. Chatterjee, P. Banerjee and R. Shyam, Nucl. Phys. **A675**, (2000) 477.
- [77] M. Zadro, Phys. Rev. C **70**, (2004) 044605.
- [78] S.C. Pieper, R.B. Wiringa and J. Carlson, Phys. Rev. C **70**, (2004) 054325.
- [79] K. Wildermuth and Y.C. Tang, *A Unified Theory of the Nucleus* (Vieweg, Braunschweig, 1977).